Fenton, C., Binnie, S. A., Dunai, T., Niedermann, S. (2022): The SPICE project: Calibrated cosmogenic 26Al production rates and cross-calibrated 26Al /10Be, 26Al/14C, and 26Al/21Ne ratios in quartz from the SP basalt flow, AZ, USA. - Quaternary Geochronology, 67, 101218.

https://doi.org/10.1016/j.quageo.2021.101218

The SPICE Project: Calibrated cosmogenic ^{26}Al production rates and cross-calibrated ^{26}Al /^{10}Be, ^{26}Al /^{14}C, and ^{26}Al/^{21}Ne ratios in quartz from the SP basalt flow, AZ, USA

Cassandra R. Fenton[*, 1, 2, 3]

Steven A. Binnie[2]

Tibor Dunai[2]

Samuel Niedermann[3]

[*]Corresponding author: E-mail: cfenton@coloradomesa.edu

[1] Present Address: Department of Physical and Environmental Sciences, Colorado Mesa University, Grand Junction, CO 81501, USA

[2] Institut für Geologie und Mineralogie, Universität zu Köln, 50674 Cologne, Germany. sbinnie@uni-koeln.de, tdunai@uni-koeln.de

[3] Deutsches GeoForschungsZentrum GFZ, Telegrafenberg, 14473 Potsdam, Germany; nied@gfz-potsdam.de

Resubmitted for publication in Quaternary Geochronology

June 29, 2021

Keywords: cosmogenic nuclide production rates, quartz, ^{26}Al, ^{26}Al/^{10}Be, ^{26}Al/^{14}C, ^{26}Al/^{21}Ne, SP lava flow

HIGHLIGHTS

- Total reference production rates at SLHL are calculated in 72 ka quartz.
- Cosmogenic ^{26}Al production rate (*St* scaling): 25.8 ± 2.5 at/g/yr (2σ).
- This rate agrees with *St* scaled production rates over past 20 ka in literature.
- The unscaled ^{26}Al/^{10}Be production ratio in 72 ka quartz is 6.7 ± 0.6 ($2\sigma_{\bar{x}}$).
- Unscaled ^{26}Al/^{14}C and ^{26}Al/^{21}Ne production ratios are 2.23±0.20 and 1.51±0.13, respectively.

ABSTRACT

The formally named SP lava flow is a quartz-, olivine- and pyroxene-bearing basalt flow that is preserved in the desert climate of northern Arizona, USA. The flow is independently dated with an ^{40}Ar/^{39}Ar age of 72±4 ka (2σ) and has undergone negligible erosion and/or burial, making its surface an ideal site for direct calibration of cosmogenic nuclide production rates. Production rates for cosmogenic ^{26}Al have been determined from SP flow quartz in this study and are combined with production rates for ^{10}Be, ^{14}C, and ^{21}Ne (Fenton et al., 2019) to yield a suite of production rate ratios. The error-weighted mean, sea-level, high latitude (SLHL) total reference production rate of ^{26}Al is 25.8 ± 2.5 at/g/yr ($2\sigma_{\bar{x}}$; standard error) using time-independent Lal (1991)/Stone (2000) (*St*) scaling factors. The *St* scaled spallogenic ^{26}Al rate is 25.0 ± 2.4 at/g/yr integrated over the past 72 ka. This rate overlaps within 2σ uncertainty with other *St*-scaled production rates in the literature. SLHL spallogenic ^{26}Al production rates in SPICE quartz (**S**P Flow **P**roduction-Rate **I**nter-Calibration Site for **C**osmogenic-Nuclide **E**valuations) are nominally lower if time-dependent *Sf*, *Sa*, and *Lm* scaling factors are used, yielding values of 22.9 ± 2.2 at/g/yr, 22.6 ± 2.2 at/g/yr, and 24.1 ± 2.2 at/g/yr ($2\sigma_{\bar{x}}$), respectively.

All ^{26}Al production rates in SP flow quartz overlap within 2σ uncertainty, regardless of time independent or time dependent scaling. Production rate ratios for cosmogenic ^{26}Al /^{10}Be, ^{26}Al /^{14}C, and ^{26}Al/^{21}Ne are based on the total, local production rates of each cosmogenic nuclide, independent of scaling models, and have error-weighted means (± $2\sigma_{\bar{x}}$; standard error) of 6.7 ± 0.6, 2.23 ± 0.20, and 1.51 ± 0.13, respectively. This study suggests that, similar to cosmogenic ^{21}Ne and ^{10}Be production rates in SP flow quartz, production rates of cosmogenic ^{26}Al in quartz do not significantly increase when integrated over 72 ka, a time span which includes the period of decreased magnetic strength from 20 to 50 ka.

1. Introduction

Cosmogenic ^{26}Al, ^{21}Ne, ^{14}C, and ^{10}Be are all produced and retained in quartz (Gosse and Phillips, 2001). Each of these nuclides, or combinations of these nuclides are commonly used in Earth-surface studies to: (1) reconstruct histories of glaciers and/or ice sheets; (2) date river gravels; (3) date buried soils or sediment; (4) determine provenance and migration of sediment in sand dunes; (5) determine production and transport rates of soil; (6) determine erosion rates of bedrock; (7) study catchment-wide denudation rates; (8) estimate recurrence intervals along faults; and (9) study paleoaltimetry (e.g., Summerfield et al., 1999; Hetzel et al., 2002; Tschudi et al., 2003; Ivy-Ochs et al., 2006, 2007; Kober et al., 2007, 2009, 2011; Balco et al., 2014; Codilean et al., 2014; Kounov et al., 2015; McPhillips et al., 2016; Blard et al., 2019). Surface-process studies employing paired cosmogenic ^{26}Al and ^{10}Be concentrations in quartz have been commonly used since the 1990s (e.g., Brown et al., 1991; Bierman and Turner, 1995; Brook et al., 1995;

82 Anderson et al., 1996; Larsen, 1996; Repka et al., 1997; Cockburn et al., 1999; Gosse and
83 Phillips, 2001; Granger et al., 2001; Schaller et al., 2001; Zehfuss et al., 2001; Schildgen
84 et al., 2002; Granger, 2006; Glasser et al., 2012; Rolfe et al., 2012). Since the advent of
85 in-situ ^{14}C measurements in quartz (Lal and Jull, 2001), it has become more common to
86 see studies that pair cosmogenic ^{14}C and ^{10}Be (Fülöp et al., 2015; Young et al., 2018;
87 Hippe et al., 2019; Skov et al., 2019), as well as studies that use a combination of three or
88 more of these four cosmogenic nuclides produced in quartz (e.g., Tschudi et al., 2003;
89 Miller et al., 2006; Balco and Shuster, 2009; Di Nicola et al., 2009; Goethals et al., 2009;
90 Kober et al., 2009; Altmaier et al., 2010; Vermeesch et al., 2010; Hippe et al., 2010,
91 2012; White et al., 2011; Briner et al., 2014; Gärtner et al., 2020).
92 In spite of the growing interest in geochronological applications of multiple *in situ*-
93 produced cosmogenic nuclides, the most commonly measured nuclide pair is still ^{10}Be
94 and ^{26}Al in quartz (Binnie et al., 2019). Estimates for cosmogenic $^{26}Al/^{10}Be$ production-
95 rate ratios in quartz range from 5.87 ± 0.24 to 7.76 ± 0.49 (Table SD1) and were
96 determined by Klein et al. (1986), Nishiizumi et al. (1989), Lal (1991), Nishiizumi et al.
97 (1991), Brown et al. (1991), Reedy et al. (1994), Larsen (1996), Kubik et al. (1998),
98 Nishiizumi et al. (2005), Goethals et al. (2009), Phillips et al. (2016), Corbett et al. (2017)
99 and Luna et al. (2018). Lal (1991) adopted the $^{26}Al/^{10}Be$ value of 6.1, which was later
100 refined to a value of 6.75 in 2010 based on improvements made in primary AMS
101 (accelerator mass spectrometry) standards (Nishiizumi et al., 2007) and the ^{10}Be half-life
102 (Chmeleff et al., 2010; Korschinek et al., 2010). The $^{26}Al/^{10}Be$ ratio of 6.75 is the
103 nominal, global value based on the KNSTD07 standardization for ^{10}Be and KNSTD
104 standardization for ^{26}Al of Nishiizumi et al. (2007) commonly used by geoscientists in

105 cosmogenic nuclide studies and is currently employed in the online calculator of Balco et
106 al. (2008).
107 The CRONUS-EU and CRONUS-Earth research networks were devised to
108 systematically re-evaluate and add to current scaling schemes and to the global network
109 of production-rate determinations, include those of cosmogenic ^{26}Al, ^{21}Ne, ^{14}C and ^{10}Be
110 in quartz (Phillips et al., 2016). The SPICE Project grew of out CRONUS-EU studies
111 (Fenton et al., 2013; Fenton and Niedermann, 2014) at the formally named SP lava flow
112 in northern Arizona, USA (Figure 1). Fenton et al. (2013) established the independent
113 ^{40}Ar/^{39}Ar age of 72±4 ka (2σ; ± 5.6%) of the SP flow. Fenton et al. (2019) presented the
114 first set of cross-calibrated cosmogenic ^{21}Ne, ^{14}C, and ^{10}Be production rates measured in
115 ten SPICE quartz samples extracted from the surface of the SP basalt flow and based on
116 this independent age.
117 Here, we present new calibrated ^{26}Al production rates and measured production-rate
118 ratios for cosmogenic ^{26}Al/^{10}Be, ^{26}Al/^{14}C, and ^{26}Al/^{21}Ne from the same ten samples of
119 SPICE quartz. This paper is the second of several papers planned to present data from the
120 SPICE project. The SPICE Project will yield a complete set of measured and cross-
121 calibrated production rates for cosmogenic ^{3}He, ^{10}Be, ^{14}C, ^{21}Ne, ^{26}Al, and ^{36}Cl in quartz,
122 olivine, and pyroxene. The project will also yield inter-calibrated production-rate ratios of
123 these commonly used cosmogenic nuclides in these three co-existing minerals.
124
125

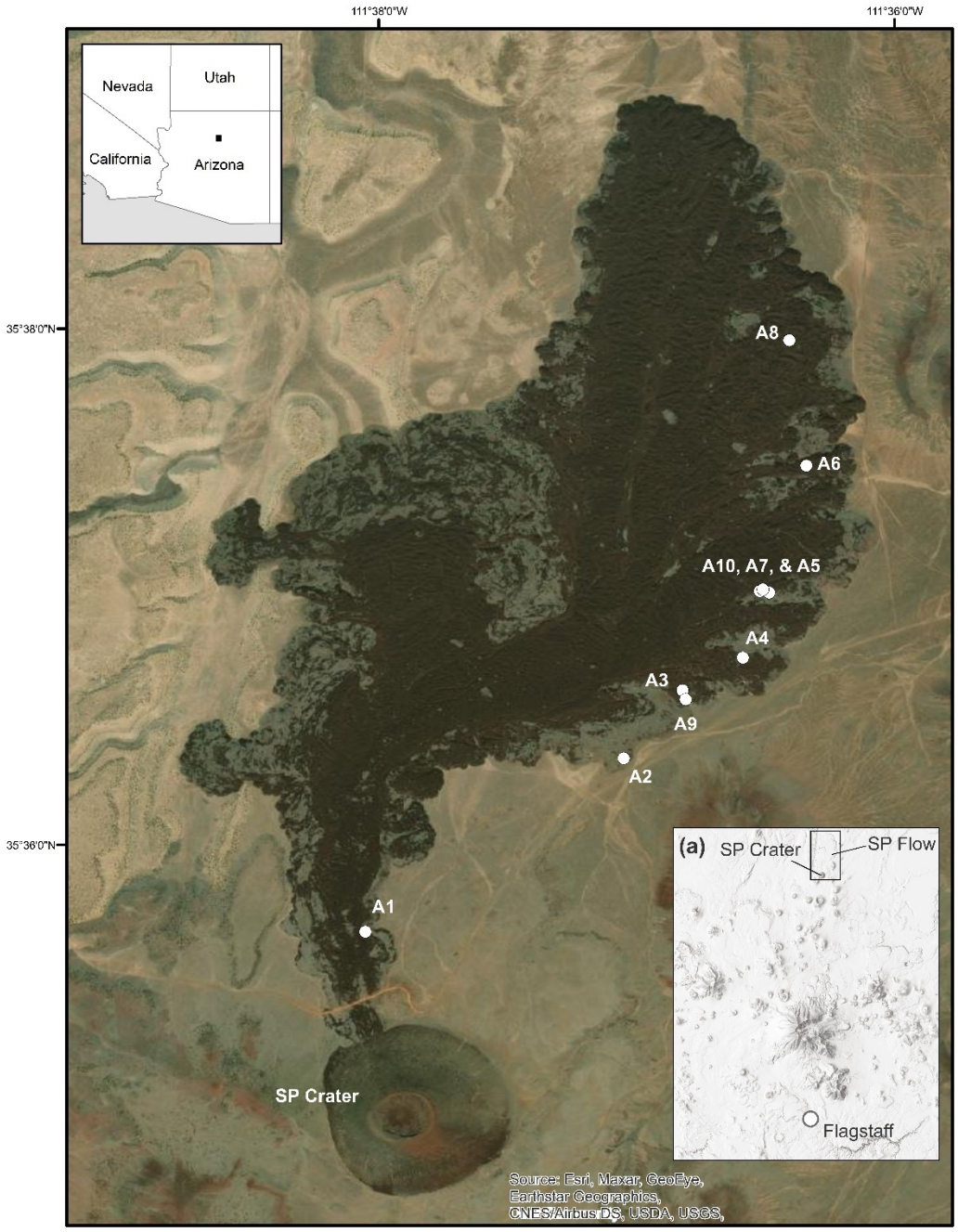

126

127 Figure 1. Satellite image of the SP lava flow and its cinder cone (SP Crater) in the
128 northern part of the San Francisco volcanic field, near Flagstaff, Arizona (inset figure
129 (a)). White circles indicate locations of SPICE sample sites (Table 1; modified after
130 Fenton et al., 2019). An interactive Google Earth map is also available in the
131 Supplementary Data of Fenton et al. (2019), where it is possible to zoom in on specific
132 sample sites.

Table 1. Sampling locations and sample types collected from the SP lava flow and SP Crater in the San Francisco volcanic field in northern Arizona, USA. An interactive Google Earth map is available in the Supplementary Data of Fenton et al. (2019).

Location/ Sample	Latitude (ºN)	Longitude (ºW)	Elev. (m)	Collected rock mass (kg)	Maximum sample thickness (cm)	Bulk whole-rock density (g/cm^3)[a]	Dip (°)	Dip azimuth (°)	Topographic shielding factor[b]	Sample thickness shielding factor[c]	Total shielding factor[d]	Pre-acid etching quartz mass[e](g)	Quartz mass used in ^{26}Al analysis (g)[f]
SPICE-													
A1	35.5944	111.6342	1837	19.1	8	2.25	0	n/a	0.999	0.946	0.945	6.10	2.1608
A2	35.6056	111.6175	1807	30.5	8	2.26	0	n/a	0.999	0.946	0.945	5.39	2.0707
A3[h]	35.6100	111.6137	1810	24.1	13	2.15	0	n/a	0.999	0.918	0.917	8.16	2.0711
													2.0559
A4[h]	35.6121	111.6098	1803	30.9	13	2.13	12	45	0.998	0.918	0.916	10.09	2.1188
													2.0803
A5	35.6163	111.6081	1800	26.8	13	2.28	0	n/a	1.000	0.913	0.913	8.53	2.1358
A6[h]	35.6245	111.6057	1778	29.5	12	2.29	0	n/a	1.000	0.919	0.919	7.35	2.0919
													2.1112
A7	35.6164	111.6087	1800	25.9	13	2.45	0	n/a	1.000	0.907	0.907	6.78	2.0676
A8[h]	35.6326	111.6068	1778	25.0	13	2.05	15	38	0.997	0.921	0.918	12.19[g]	2.1391
													2.1340
A9	35.6094	111.6135	1810	30.5	13	2.29	0	n/a	0.999	0.912	0.912	8.49	2.0503
A10	35.6165	111.6085	1800	25.0	12	2.31	7	315	0.999	0.918	0.917	5.32	2.0525

Note: All SPICE samples were collected in 2015 from the exposed surfaces of pressure ridges on the SP lava flow. n/a = not applicable or not available.

[a] Bulk densities were measured for each sample.

[b] Calculated using CRONUSCalc Topographic Shielding Calculator version 2.0 (Marrero et al., 2016).

[c] Calculated using CRONUS-EU CosmoCalc version 3.0 (Vermeesch, 2007) with the bulk whole-rock density measured or reported for each sample and an exponent of topographic shielding correction of 2.3.

[d] The total shielding factor includes corrections for sample depth (self-shielding) and topographic shielding, which includes dipping of a sample site surface, when present. Shielding factor = 1.0 equates to no shielding correction.

[e] Samples yielded quartz concentrates (>75% quartz) in the 125-1000 µm fraction, unless otherwise noted. Masses reported here are the amounts of quartz extracted from each basalt sample prior to any treatment with HF acid.

[f] ^{10}Be was extracted from these same quartz masses (Fenton et al., 2019).

[g] Sample yielded quartz concentrates in the 90-1000 µm fraction.

[h] Sufficient purified quartz was obtained to allow duplicate sample preparation and ^{26}Al measurement. Listed masses are those used in duplicate sample preparation and AMS measurements

2. Current Values of SLHL Production Rates for ^{26}Al in Quartz

Geoscientists use a variety of scaling factors to calculate sea-level, high-latitude (SLHL) total reference production rates, spallation production rates, and muon-induced production rates of cosmogenic nuclides, such as ^{10}Be, ^{14}C, ^{21}Ne, and ^{26}Al (see sections 6.3.1 and 6.3.2 for more details on each type of production rate). Until recently, the combined Lal (1991)/Stone (2000) model (*St*) has been the most commonly used scaling method. The *St* model is time-independent and calculates a constant scaling factor for a given latitude and elevation, thus, *St* scaling-factor values are a function of the geographic position of a sample site. The time-dependent models *Sf* and *Sa* were developed by Lifton et al. (2014) and account for documented temporal variations in the strength of the geomagnetic field. *Sf* scaling factors can be used with any cosmogenic nuclide, whereas *Sa* scaling factors are nuclide specific. The time dependent *Lm* scaling method (as denoted by Balco et al., 2008) is based on the *St* model of Lal (1991)/Stone (2000) and is modified for geomagnetic corrections as described in Nishiizumi et al. (1989).

SLHL production rates of cosmogenic ^{26}Al in quartz are reported by Nishiizumi et al. (1989), Lal (1991), Brown et al. (1991), Brook et al. (1996), Kubik et al. (1998), Kelly et al. (2015), Lifton et al. (2015), Borchers et al. (2016), and Luna et al. (2018). SLHL production rates from studies conducted between 1989 and 1998 range from 34 to 36.8 at/g/yr and are excluded from the calibrated ^{26}Al production rate determined by the CRONUS-Earth Project (Borchers et al., 2016). Their calibration data set includes only three sites determined to be the highest quality sites that had been studied up until 2010. These spallation production rates are used in the frequently used online calculators of

Balco et al. (2008; version 3.0) and Marrero et al. (2016; CRONUSCalc). The samples used for Borchers et al.'s (2016) ^{26}Al calibration data set are a subset of their full cosmogenic ^{10}Be spallation production-rate data set that also had accompanying ^{26}Al measurements in the same quartz samples. The calibrated spallation production rate of ^{26}Al of Borchers et al. (2016) combines data from the following primary calibration sites: Promontory Point, Utah, USA (PPT; 18.3 ka), Isle of Skye, Scotland (SCOT; 11.7 ka), and Quelccaya, Peru (PERU; 12.2 ka) (Kelly et al., 2015; Lifton et al., 2015; Borchers et al., 2016). The SLHL spallogenic ^{26}Al production rates scaled with the *St*, *Sf*, and *Sa* methods and reported in Borchers et al. (2016) are 27.9, 28.6, and 28.5 at/g/yr, respectively (Table 2). No uncertainties are reported with the rates, because Borchers et al. (2016) state they "cannot infer statistically justifiable production rate uncertainties from the fitting exercise".

Table 2. Spallation ^{26}Al production rates in quartz reported by Borchers et al. (2016) and those presented in this study (see section 6 for presentation of results).

Cosmogenic nuclide	SLHL spallation production rate *St* (at/g/yr)	SLHL spallation production rate *Sf* (at/g/yr)	SLHL spallation production rate *Sa* (at/g/yr)
$^{26}Al_{sp}$ (Borchers et al., 2016)	27.9	28.6	28.5
SPICE $^{26}Al_{sp} \pm 2\sigma_{\bar{x}}$ [a] (see section 6)	25.0 ± 2.4	22.9 ± 2.2	22.6 ± 2.2
SPICE $^{26}Al_{sp} \pm 2\sigma_{SD}$ [b] (see section 6)	25.0 ± 1.9	23.0 ± 1.8	22.7 ± 1.8

Note: *St* refers to the time-independent scaling method of Lal (1991)/Stone (2000). *Sf* and *Sa* refer to the time-dependent scaling methods of Lifton et al. (2014) for non-nuclide specific and nuclide specific factors, respectively. The subscript *sp* refers to a production rate induced by spallation reactions.

[a] This is the **error-weighted mean and two standard errors ($2\sigma_{\bar{x}}$)** of the mean for all samples and includes the uncertainty of the ^{40}Ar/^{39}Ar age.

[b] This is the arithmetical mean and two standard deviations ($2\sigma_{SD}$) of all samples; $2\sigma_{SD}$ does not include uncertainty of the ^{40}Ar/^{39}Ar age.

194 Using cosmogenic ^{26}Al data from the three primary calibration sites (PPT, SCOT, and
195 PERU), as listed in the ICE-D Production Rate Calibration Data database
196 (http://calibration.ice-d.org/), SLHL production rates were calculated in this study using
197 the online calculator of Balco et al. (2008; https://hess.ess.washington.edu/) to make them
198 more directly comparable to the SPICE production rates calculated in the same version of
199 the calculator. The production rates of spallogenic ^{26}Al range from 26.5 ± 2.6 to 31.7 ±
200 4.4 at/g/yr ($2\sigma_{SD}$), when scaled with the *St* scaling method. The same calculator yields
201 production rates of spallogenic ^{26}Al ranging from 28.2 ± 6.0 to 31.7 ± 4.4 at/g/yr ($2\sigma_{SD}$;
202 Table 3; Figure 2) when scaled with the *Lm* scaling method. The above production rates
203 are reported as arithmetical means with associated two standard deviations ($2\sigma_{SD}$).
204 Combining ICE-D data from all three calibration sites in the Balco et al. (2008) calculator
205 and using the *St* and *Lm* scaling methods yields SLHL spallation production rates of 30.0
206 ± 6.0 to 30.5 ± 5.6 at/g/yr ($2\sigma_{SD}$), respectively. This *St*-scaled value is greater than the *St*-
207 scaled value reported by Borchers et al. (2016; 27.9 at/g/yr; Table 2), but the values agree
208 within uncertainty. Presumably, the discrepancy in values is related to the differences in
209 calculations and/or coding algorithms by the two sets of authors.
210 Argento et al. (2015a) report a SLHL spallogenic ^{26}Al production rate of 29.6 ± 4.4
211 at/g/yr. This value is based on a nuclear-physics based model that combines transport
212 modeling with excitation functions for commonly measured cosmogenic nuclides,
213 including ^{26}Al. This modeled SLHL spallogenic ^{26}Al production rate agrees well with
214 calibrated ^{26}Al production rates of Borchers et al. (2016) listed above.
215
216

Table 3. Comparison of spallation ^{26}Al production rates in SPICE quartz to rates calculated based on the primary-calibration data set for ^{26}Al production rates (Borchers et al., 2016) in the ICE-D Production Rate Calibration Data database (http://calibration.ice-d.org/). Rates are reported as **arithmetical means with two standard deviations ($2\sigma_{SD}$) as calculated in the online calculator of Balco et al. (2008).**

Cosmogenic nuclide	SLHL production rate ± $2\sigma_{SD}$ *St* (at/g/yr) [a]	SLHL production rate ± $2\sigma_{SD}$ *Lm* (at/g/yr) [a]
SPICE $^{26}Al_{sp}$	25.2 ± 2.2	24.4 ± 2.2
Combined $^{26}Al_{sp}$ data from PPT, SCOT, and PERU primary calibration sites of Borchers et al. (2016)	30.0 ± 6.0	30.5 ± 5.6
SCOT $^{26}Al_{sp}$	31.7 ± 4.4	31.7 ± 4.4
PPT $^{26}Al_{sp}$	28.1 ± 6.0	28.2 ± 6.0
PERU $^{26}Al_{sp}$	26.5 ± 2.6	29.1 ± 3.0

Note: Uncertainty is reported here as two standard deviations ($2\sigma_{SD}$) according to online documentation (Balco, 2017). The subscript *sp* refers to a production rate produced by spallation reactions. *St* refers to the time-independent scaling method of Lal (1991)/Stone (2000). *Lm* refers to the time dependent scaling method of Lal (1991)/Stone (2000) as corrected for paleomagnetic variations described in Nishiizumi et al. (1989) and denoted as *Lm* by Balco et al. (2008).

[a] Online calculator of Balco et al. (2008); Version 3 of production-rate calibration code: wrapper 3.0.2; get_age 3.0.2; muons 1A, alpha = 1; validate_v3_input.m – 3.0; consts 3.0.4

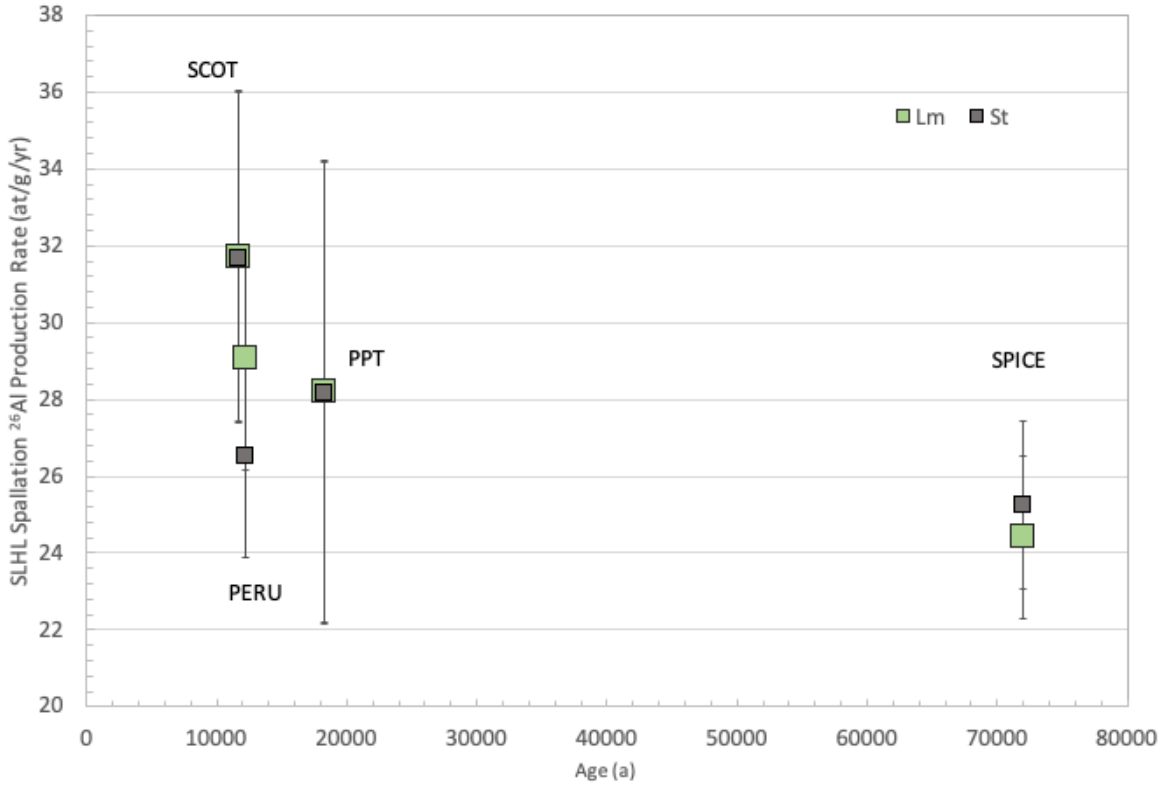

Figure 2. Comparison of the arithmetical mean ^{26}Al production rates of the SPICE study with those of Lifton et al. (2014; PPT), Kelly et al. (2015; PERU) and Borchers et al. (2016; SCOT) as calculated in the online calculator of Balco et al. (2008) using both the *St* and *Lm* scaling methods. Error bars represent $2\sigma_{SD}$ (standard deviations).

3. ^{26}Al-Based Production Rate Ratios in Quartz

While estimates for cosmogenic ^{26}Al/^{10}Be production-rate ratios in quartz range from 5.87 ± 0.24 to 7.76 ± 0.49 in multiple studies (Table SD1 including references; Figure 3), mean cosmogenic ^{26}Al/^{10}Be ratios range from 6.53 to 7.19 in quartz from the three primary ^{26}Al calibration sites of Borchers et al. (2016; PPT, SCOT, and PERU).

There is no agreement between the ^{26}Al/^{10}Be ratios in quartz from the SCOT and PPT calibration sites, however, the ^{26}Al/^{10}Be ratios measured in quartz from the PERU site overlaps both ^{26}Al/^{10}Be values from PPT and SCOT quartz (Figure 3). The arithmetical

mean $^{26}Al/^{10}Be$ values at the PPT and SCOT primary calibration sites are 6.53 ± 0.14 and 7.19 ± 0.18 ($2\sigma_{SD}$), respectively, based on calculations made in this study with data from Borchers et al.'s (2016) primary-calibration data sets for ^{26}Al and ^{10}Be data. The data are listed in the ICE-D Production Rate Calibration Data database (http://calibration.ice-d.org/). Phillips et al. (2016) report a $^{26}Al/^{10}Be$ ratio of 6.74 ± 0.34 (2σ) for the PERU site (Table SD1). The $^{26}Al/^{10}Be$ ratios measured in quartz from the PPT and PERU sites are in strong agreement and agree well with the commonly accepted $^{26}Al/^{10}Be$ value of 6.75.

Cross-calibrated cosmogenic $^{26}Al/^{14}C$ and $^{26}Al/^{21}Ne$ production-rate ratios have been determined in quartz from calibration sites where ^{14}C, ^{21}Ne, and ^{26}Al were measured in the same quartz samples. Based on data reported in Lifton et al. (2015) for the PPT site, error-weighted mean and arithmetical mean $^{26}Al/^{14}C$ ratios of 1.93 ± 0.05 ($2\sigma_{\bar{x}}$) and 1.90 ± 0.33 ($2\sigma_{SD}$) were calculated in that study (Table SD2). Cosmogenic ^{21}Ne was not measured in quartz from the PPT site. Neither cosmogenic ^{21}Ne nor cosmogenic ^{14}C were measured in quartz from either the PERU or SCOT calibration sites, thus neither $^{26}Al/^{21}Ne$ nor $^{26}Al/^{14}C$ values are reported for those sites. Goethals et al. (2009) report a $^{26}Al/^{21}Ne$ production ratio of 1.80 ± 0.09 (2σ) in quartz from the Bishop Tuff in California, USA. Niedermann et al. (1994) and Balco and Shuster (2009) report $^{26}Al/^{21}Ne$ ratios of 1.65 ± 0.28 and 1.65 ± 0.15, respectively. Cosmogenic ^{14}C was not measured in quartz during the studies of Goethals et al. (2009), Niedermann et al. (1994), and Balco and Shuster (2009), thus, $^{26}Al/^{14}C$ values are not reported for those sites.

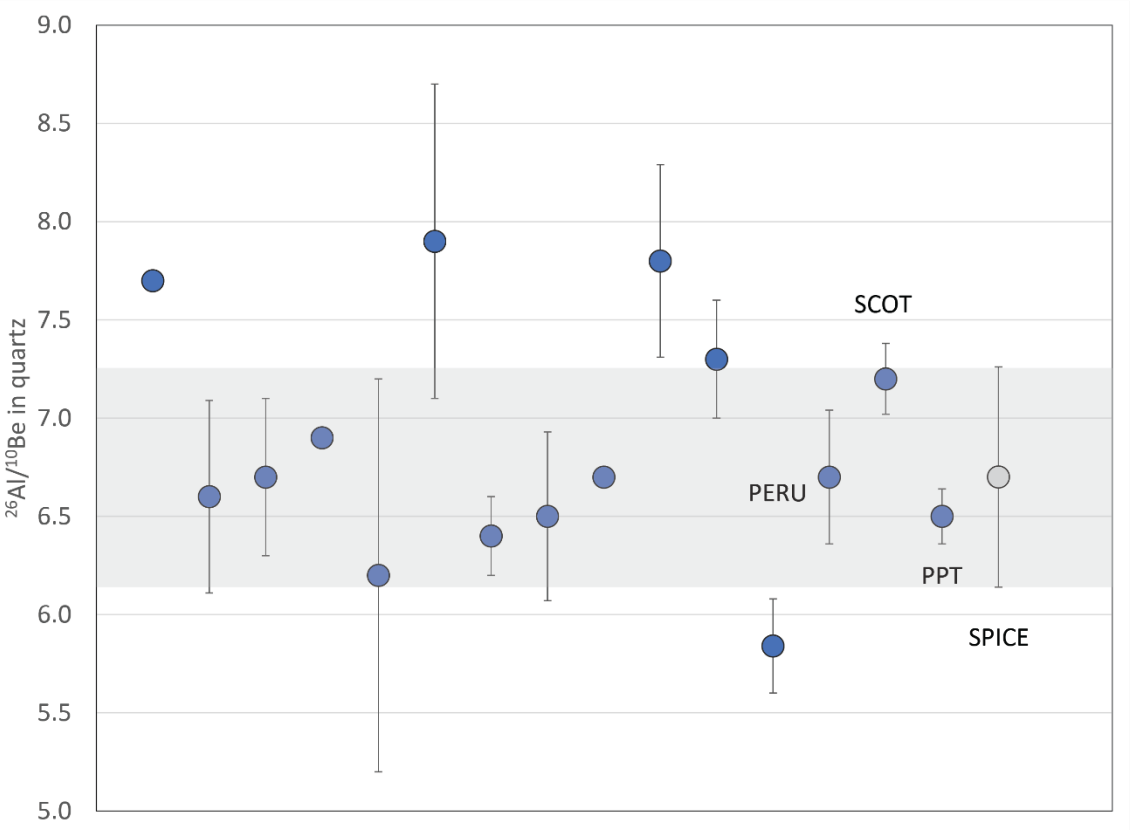

Figure 3. Comparison of previously published $^{26}Al/^{10}Be$ values in quartz (blue circles). Error bars represent 2σ uncertainty. References and $^{26}Al/^{10}Be$ ratios are listed in Table SD1. The gray circle represents the $^{26}Al/^{10}Be$ ratio based on the local production rates of cosmogenic ^{26}Al and ^{10}Be in quartz from SPICE samples. PPT, SCOT, and PERU values are from primary calibration studies in Borchers et al. (2016). The shaded rectangle represents 2σ uncertainty of the error-weighted mean SPICE $^{26}Al/^{10}Be$ ratio.

Based on SLHL production rates of spallogenic ^{26}Al, ^{21}Ne, ^{14}C, and ^{10}Be in quartz listed in Borchers et al. (2016), $^{26}Al_{sp}/^{21}Ne$ $^{26}Al_{sp}/^{14}C_{sp}$, and $^{26}Al_{sp}/^{10}Be_{sp}$ values are 1.68, 2.28, and 6.97, respectively, using the *St* scaling method (Table SD3). Here, the subscript *sp* refers to the spallogenic portion of total production rates of a given cosmogenic nuclide (see section 6.3.2). Fenton et al. (2019) make no distinction between total reference and spallation production rates of ^{21}Ne, hence no subscript *sp*, based on the studies of Balco and Shuster (2009), Goethals et al. (2009), Kober et al. (2011) and Balco et al. (2019). These latter studies indicate muogenic contributions to the total ^{21}Ne

284 production rate should come only from fast muon interactions and that negative muon
285 capture is negligible. Values for $^{26}Al_{sp}/^{21}Ne$, $^{26}Al_{sp}/^{14}C_{sp}$, and $^{26}Al_{sp}/^{10}Be_{sp}$ based on *Sf* and
286 *Sa* scaling models are also calculated (Table SD3). Uncertainties are not reported with the
287 Borchers et al. (2016) data, thus, no uncertainties are calculated for the above ratios.
288 These ratios appear to agree well with other published $^{26}Al/^{21}Ne$, $^{26}Al/^{14}C$, and $^{26}Al/^{10}Be$
289 values listed above.
290 Based on the modeled SLHL production rates of spallogenic ^{26}Al, ^{21}Ne, ^{14}C, and ^{10}Be
291 in quartz reported in Argento et al. (2015a), $^{26}Al_{sp}/^{21}Ne$, $^{26}Al_{sp}/^{14}C_{sp}$, and $^{26}Al_{sp}/^{10}Be_{sp}$
292 values are 2.43, 1.96, and 6.7, respectively, using their own scaling method (Table 4).
293 Uncertainties are reported with the Argento et al. (2015a) data, but it is not specified
294 whether they are 1σ or 2σ. These $^{26}Al/^{14}C$ and $^{26}Al/^{10}Be$ ratios also appear to generally
295 agree with other published values listed above. The $^{26}Al/^{21}Ne$ ratios of Argento et al.
296 (2015a) overlap within uncertainty with $^{26}Al/^{21}Ne$ ratios of Borchers et al. (2016) and
297 Niedermann et al. (1994); however, $^{26}Al/^{21}Ne$ ratios of Argento et al. (2015a) are greater
298 than the $^{26}Al/^{21}Ne$ ratios of Balco and Shuster (2009) and Goethals et al. (2009).
299 **4. Geologic Background on the SP basalt flow**
300 Description of the SP flow relevant to the SPICE project was first presented by
301 Fenton et al. (2019). Here, we summarize again the important highlights relevant to
302 interpretation of cosmogenic ^{26}Al production rates in the surface of the flow.
303 The SP lava flow is a basaltic andesite located in the San Francisco volcanic field of
304 northern Arizona (Billingsley et al., 2007), approximately 55 km north of Flagstaff, AZ
305 (Figure 1a). The basalt has well-preserved primary flow features, including lava-flow
306 levees, aa, pressure ridges, and agglutinate features. Most of the lava-flow surface is free

of desert-pavement and/or soil formation (Fenton and Niedermann, 2014), and appears as the black areas in satellite image (Figure 1).

The independently dated, quartz-bearing, and well-preserved SP flow creates a fortuitous opportunity to study cross-calibrated cosmogenic production rates. The flow has a radiometric age of 72±4 ka (2σ; ± 5.6%) based on $^{40}Ar/^{39}Ar$ analysis of three basalt groundmass samples (Fenton et al., 2013). The $^{40}Ar/^{39}Ar$ age is in excellent agreement with a previously reported K-Ar age (70±8 ka; Baksi, 1974). The lava flow

Table 4. Comparison of average SLHL spallation production rates and resultant production-rate ratios reported in Argento et al. (2015a) and Fenton et al. (2019 and this study).

	Argento et al. (2015a) SLHL SPR (at/g/yr)	Uncer-tainty [a]	SPICE Balco *St* SLHL SPR (at/g/yr) [b,c]	$2\sigma_{SD}$ [b,c]	SPICE Balco *Lm* SLHL SPR (at/g/yr) [b,c]	$2\sigma_{SD}$ [b,c]	SPICE *St* SLHL SPR (at/g/yr) [c]	$2\sigma_{SD}$ [c]	SPICE *Sf* SLHL SPR (at/g/yr) [c]	$2\sigma_{SD}$ [c]	SPICE *Sa* SLHL SPR (at/g/yr) [c]	$2\sigma_{SD}$ [c]
$^{10}Be_{sp}$	4.41	0.66	3.73	0.20	3.61	0.20	3.75	0.18	3.45	0.13	3.31	0.16
$^{14}C_{sp}$	15.1	2.3	9.1	3.4	9.6	3.6	9.2	1.7	9.5	1.7	9.6	1.7
^{21}Ne	12.2	1.8	16.5	2.0	16.0	2.0	16.7	2.1	15.3	1.9	n/a	n/a
$^{26}Al_{sp}$	29.6	4.4	25.2	2.2	24.4	2.2	25.0	1.9	23.0	1.8	22.7	1.8
$^{26}Al_{sp}/^{10}Be_{sp}$	6.7	1.4	6.8	0.7	6.8	0.7	6.7	0.7	6.7	0.7	6.9	0.7
$^{26}Al_{sp}/^{14}C_{sp}$	1.96	0.42	2.77	1.06	2.54	0.98	2.67	0.29	2.39	0.29	2.35	0.29
$^{26}Al_{sp}/^{21}Ne$	2.43	0.51	1.53	0.23	1.53	0.24	1.46	0.14	1.50	0.15	n/a	n/a

Note: SPR refers to "spallation production rate". *St* refers to the time-independent scaling method of Lal (1991)/Stone (2000). *Lm* refers to the time dependent scaling method of Lal (1991)/Stone (2000) as corrected for paleomagnetic variations described in Nishiizumi et al. (1989) and denoted as *Lm* by Balco et al. (2008). *Sf* and *Sa* refer to the time-dependent scaling methods of Lifton et al. (2014) for non-nuclide specific and nuclide specific factors, respectively. The subscript *sp* refers to a production rate induced by spallation reactions.

[a] Type of uncertainty (standard deviation or standard error) was not specified in Argento et al. (2015a), nor was it specified if uncertainty is reported as 1σ or 2σ.

[b] Values calculated in the online calculator of Balco et al. (2008) in this study and in Fenton et al. (2019) reported as arithmetical mean and two standard deviations ($2\sigma_{SD}$) of all samples

[c] This is the arithmetical mean and two standard deviations ($2\sigma_{SD}$) of all samples as reported in Table 2 in both this study and Fenton et al. (2019); $2\sigma_{SD}$ does not include uncertainty of the $^{40}Ar/^{39}Ar$ age of the SP flow.

contains evenly distributed quartz xenocrysts (not xenoliths) co-existing with olivine and pyroxene phenocrysts. This is a relatively rare occurrence, because quartz does not

usually crystallize in basaltic lavas. The youthful, unweathered appearance of the flow's surface and the lack of soil development indicate negligible erosion. Fenton et al. (2019) calculated that erosion rates of 0.2 – 53 mm/kyr would be required to account for differences between SLHL production rates of cosmogenic ^{10}Be, ^{14}C, and ^{21}Ne in SPICE quartz and SLHL production rates for the same nuclides reported by Borchers et al. (2016); however, these erosion rates would result in 1.4 – 310 cm of surface erosion. Abundant field evidence does not support this degree of erosion, and demonstrates that erosion on the order of 10^1 – 10^2 cm over the past 72 ka is unrealistic (see field photographs in the Supplemental Data of Fenton et al. 2019). Areas along the edges of the flow, mainly on the western side, do have occasional, well-developed patches of desert pavements overlying the fine-grained A soil horizon (A_v; 10-15 cm deep; McFadden et al., 1998). These patches are the gray-to-green colored areas in the satellite image of the SP lava flow (Figure 1). SPICE Project sample sites are located on the surfaces of well-preserved pressure ridges (Figures 1 and 4; Table 1). Additional photographs of sample sites on the SP flow can be found in the Supplementary Material of Fenton et al. (2019).

Figure 4. Photograph of a representative pressure ridge at the SP lava flow. The small whiteboard in the distance stands 22 cm tall and is on the surface from which SPICE-A9 was collected. Notice the well-developed desert varnish and the continuity of the pressure-ridge surfaces, indicating negligible erosion.

5. Methods

5.1 SPICE sample collection, shielding corrections and quartz separation

Surface samples in this study were collected from the SP lava flow in 2015. The concentration of evenly distributed quartz xenocrysts in the basalt is quite low (<2-3%;

Rittenour et al., 2012). Thus, between 19 and 31 kg of basalt were collected for samples SPICE-A1 through –A10 (Table 1). All samples were collected from the well-preserved surfaces of pressure ridges on the SP lava flow. Photographs of sample sites can be found in the Supplementary Data section of Fenton et al. (2019). Elevations of sample sites ranged from 1778 m to 1837 m, and sample thicknesses ranged from 8 cm to 13 cm (Table 1). Corrections were made to production rates based on topographic shielding and self-shielding (i.e., dipping of a boulder surface and/or sample thickness) according to CRONUSCalc Topographic Shielding Calculator version 2.0 (Marrero et al., 2016) and CosmoCalc (Vermeesch, 2007). A value of 2.3 was used for the exponent *m* in Equation 3 of Vermeesch (2007). Bulk whole-rock densities (2.05-2.45 g/cm^3) were measured and used in calculation of the self-shielding factor (Table 1).

Standard techniques were used to prepare samples for analysis. Whole-rock samples were crushed, washed, and sieved. Quartz was concentrated for each sample from the 90-125, 125-250, 250-500, 500-710 and 710-1000 μm grain-size fractions. Details of magnetic and density separations for samples SPICE-A1 through A10 are reported in Fenton et al. (2019). Quartz concentrates were treated and purified according to procedures introduced by Kohl and Nishiizumi (1992). Details are given in Fenton et al. (2019). Splits of purified quartz were taken from each sample for measurement of cosmogenic ^{26}Al, ^{21}Ne, ^{14}C, and ^{10}Be. Cosmogenic ^{26}Al and ^{10}Be were extracted from the same purified quartz split for each sample (SPICE-A1 through –A10).

5.2 Al extraction and AMS analysis

Around two grams of purified quartz was dissolved for each of samples SPICE-A1 to -A10, after being spiked with ~250 μg of a commercial beryllium solution (Scharlab,

1000 mg/l, density 1.02 g/cm^3) and ~1.5 mg of a commercial aluminum solution (Scharlab, 1000 mg/l, density 1.03 g/cm^3) (Tables 1 and SD4). From four of the samples (SPICE-A3, -A4, -A6 and -A8) there was enough quartz extracted to allow duplicate sample preparation. Laboratory preparation of the purified quartz as AMS targets was undertaken in the clean laboratories at the University of Cologne in two batches of eight samples, each batch additionally containing two reagent blanks and a CoQtz-N quartz reference sample (Binnie et al., 2019). Following dissolution and dry down, sample residue was heated in the presence of aqua regia to decompose insoluble AlF salts and an aliquot was taken for determination of aluminum by standard addition (n=4) using in-house ICP-OES (Inductively Coupled Plasma – Optical Emission Spectroscopy). The ICP-OES measurements were performed on all samples and blanks in tandem with quality control measurements of NIST SRM165a. Aluminum was separated using the single-step column approach described by Binnie et al. (2015). Aluminum hydroxide was co-precipitated with Ag according to Stone et al. (2004), for pressing into AMS targets.

Determinations of $^{26}Al/^{27}Al$ were undertaken at CologneAMS (Dewald et al., 2013), normalized to the standard values reported by Nishiizumi (2004). Details can be found in the footnotes of table SD4. Blank corrected ^{26}Al concentrations are derived following Binnie et al. (2019). Total ^{26}Al concentrations are corrected for decay using the ^{26}Al half-life of 705 kyr (Nishiizumi, 2004).

6. Results

6.1 Cosmogenic ^{26}Al concentrations

AMS analysis of our SPICE samples yielded $^{26}Al/^{27}Al$ ratios ranging from 2.92×10^{-13} to

404 3.58×10^{-13} (Table SD4). Both batches of SPICE samples were processed in the laboratory
405 alongside a pair of blanks that gave measured $^{26}Al/^{27}Al$ values between ~3.3×10^{-15} and
406 ~7.0×10^{-15}. The arithmetic mean of ^{26}Al atoms in each blank pair was subtracted from
407 the ^{26}Al atoms measured in the relevant SPICE samples, resulting in blank subtractions of
408 between 0.4% and 1.6% of the total ^{26}Al atoms measured. ^{26}Al concentration
409 measurements of quartz reference material CoQtz-N from each batch were $16.87 \pm 0.80 \times$
410 10^6 atoms/g and $15.31 \pm 0.81 \times 10^6$ atoms/g, in good agreement with the preliminary
411 consensus value estimate for this material ($15.6 \pm 1.6 \times 10^6$ atoms/g at the 95%
412 confidence limit, Binnie et al., 2019). In the case of duplicate samples (SPICE-A3, -A4, -
413 A6 and -A8) the error weighted mean ^{26}Al concentration was calculated following
414 Wilson and Ward (1978) and used for the production-rate determinations.

415 **6.2 Calculations of local production rates and production-rate ratios**

416 Cosmogenic ^{26}Al concentrations (atoms/g quartz; Table SD4) are corrected for
417 topographic and self-shielding (including sample thickness and variations in whole-rock
418 density; Table 1). Corrected, local ^{26}Al production rates (at/g/yr) are listed in Table 5 and
419 shown in Figure 5.

420 Production rates of cosmogenic ^{26}Al (Table 5) are based on the independent $^{40}Ar/^{39}Ar$
421 eruption age of the SP flow (72±4 ka; 2σ; Fenton et al., 2013). In the absence of erosion
422 or burial, the unscaled production rate of cosmogenic ^{26}Al (P_0) is related to the measured
423 concentration of ^{26}Al ($C(t)$) of a quartz sample at time (t), and the ^{26}Al decay constant (λ),
424 such that:

425 $$P_0 = \frac{\lambda C(t)}{(1-e^{-\lambda t})} \qquad \text{[Eq. 1].}$$

426 Each local production rate refers to total production (spallation production + muon

427 production) at each sample site and excludes use of scaling factors. Thus, these local
428 production rates are latitude, longitude, and elevation specific. Local production rates for
429 ^{26}Al are 86 - 94 at/g/yr in SP flow quartz and agree within 1σ uncertainty (Figure 5).
430 Local production rates of cosmogenic ^{10}Be, ^{14}C, and ^{21}Ne of Fenton et al. (2019) are
431 used in this study to calculate ^{26}Al/^{10}Be, ^{26}Al/^{14}C, and ^{26}Al/^{21}Ne ratios (Table SD5;
432 Figures 6, 7, and 8). Production rates of cosmogenic ^{21}Ne and ^{10}Be at the SP flow are also
433 directly calibrated against the ^{40}Ar/^{39}Ar eruption age (72±4 ka; 2σ; Fenton et al., 2019).
434 The production rate of cosmogenic ^{14}C (Fenton et al., 2019) is based on the assumption
435 that radioactive nuclide saturation occurred in quartz in the SP flow surface after around
436 4.5 half-lives, which equates to 25 ka. Thus, the production rates (P_0) of ^{14}C at the SP
437 flow are calculated using the equation $P_0 = \lambda C(t)$, where λ is the ^{14}C decay constant ($\lambda = \ln 2/t_{½}$, with $t_{½}$ = 5730 ± 40 yr).
439 Table SD5 lists production-rate ratios for ^{26}Al/^{10}Be, ^{26}Al/^{14}C, and ^{26}Al/^{21}Ne in
440 SPICE quartz based on the local production rates of each cosmogenic nuclide, which are
441 not yet scaled and therefore independent of scaling models. Error-weighted means ($\pm 2\sigma_{\bar{x}}$
442 standard error) of 6.7 ± 0.6, 2.23 ± 0.20, and 1.51 ± 0.13 are calculated for ^{26}Al/^{10}Be,
443 ^{26}Al/^{14}C, and ^{26}Al/^{21}Ne, respectively. Standard errors include uncertainties related to
444 measurements, corrections for shielding, the ^{40}Ar/^{39}Ar age, and the ^{14}C half-life (where
445 applicable).
446 **6.3 Scaling methods and SLHL production rates**
447 Scaling factors are used to calculate total SLHL reference production rates, spallation
448 production rates, and muon-induced production rates for ^{26}Al in SPICE quartz samples
449 (Table SD6). Ten samples (SPICE-A1 to -A10) are used in the calculations of all SLHL

450 ^{26}Al production rates. All uncertainties are reported as either standard error ($2\sigma_{\bar{x}}$) or
451 standard deviations ($2\sigma_{SD}$) and are noted accordingly. Standard errors are reported with
452 error-weighted means, and standard deviations are reported with arithmetical means.
453 *St*, *Sf*, *Sa,* and *Lm* scaling models are employed to scale cosmogenic ^{26}Al data in this
454 study (Tables 3, 4, 5, and SD6) and were used for the ^{10}Be, ^{14}C, and ^{21}Ne data presented
455 in Fenton et al. (2019). *St* scaling factors are calculated using the CRONUSCalc online
456 calculator (Marrero et al., 2016). *Sf* and *Sa* scaling factors were calculated in Matlab
457 using the mmc1 code of Lifton et al. (2014). Individual *Lm* scaling factors for each time
458 step, such as those produced from the mmc1 code (Lifton et al., 2014), are not reported

459 Table 5. Muogenic portions, spallogenic portions, and total reference SLHL ^{26}Al production rates for SPICE quartz samples.

Sample ID	Total cosmogenic ^{26}Al concentration (10^6 at/g) [a]	2σ uncertainty (10^6 at/g) [a]	Total ^{26}Al production rate at local sampling elevation (at/g/yr) [b]	2σ uncertainty (at/g/yr) [b]	^{26}Al production rate from negative muon capture at local sampling elevation (at/g/yr) [c]	2σ uncertainty (at/g/yr) [c]	Spallogenic ^{26}Al production rate at SLHL (*St*-scaled) (at/g/yr) [d,e]	2σ uncertainty (at/g/yr) [d]	Muogenic ^{26}Al production rate at SLHL (*St*-scaled) (at/g/yr) [e]	2σ uncertainty (at/g/yr)	Total reference ^{26}Al production rate at SLHL (*St*-scaled) (at/g/yr)	2σ uncertainty (at/g/yr)
SPICE-A1	6.3	1.0	89	14	1.58	0.43	24.4	5.4	0.79	0.21	25.2	5.4
SPICE-A2	6.1	0.9	86	13	1.56	0.42	24.3	5.4	0.80	0.22	25.1	5.4
SPICE-A3	6.3	1.0	89	14	1.56	0.42	24.9	5.7	0.80	0.21	25.7	5.7
SPICE-A4	6.3	1.0	89	15	1.55	0.42	25.2	6.0	0.80	0.22	26.0	6.0
SPICE-A5	6.1	1.0	86	14	1.55	0.42	24.3	5.7	0.80	0.22	25.1	5.7
SPICE-A6	6.7	1.2	94	17	1.53	0.41	27.1	7.2	0.80	0.22	27.9	7.2
SPICE-A7	5.9	1.4	84	20	1.55	0.42	23.7	8.4	0.80	0.22	24.5	8.4
SPICE-A8	6.3	1.2	89	16	1.54	0.41	25.7	6.9	0.80	0.22	26.5	6.9
SPICE-A9	6.3	1.2	90	17	1.56	0.42	25.2	6.9	0.80	0.21	26.0	6.9
SPICE-A10	6.4	1.3	90	18	1.55	0.42	25.6	7.5	0.80	0.22	26.4	7.5
						Average [f]	**25.0**	**2.4** ($2\sigma_{\bar{x}}$)	**0.80**	**0.08** ($2\sigma_{\bar{x}}$)	**25.8**	**2.5** ($2\sigma_{\bar{x}}$)

460
461

462 Table 5 (continued). Scaled with *Sf* and *Sa* scaling factors

Sample ID	Spallogenic ^{26}Al production rate at SLHL (*Sf*-scaled) (at/g/yr) [d,e]	2σ uncertainty (at/g/yr) [d]	Muogenic ^{26}Al production rate at SLHL (*Sf*-scaled) (at/g/yr) [e]	2σ uncertainty (at/g/yr)	Total reference ^{26}Al production rate at SLHL (*Sf*-scaled) (at/g/yr) [e,]	2σ uncertainty (at/g/yr)	Spallogenic ^{26}Al production rate at SLHL (*Sa*-scaled) (at/g/yr) [d,e]	2σ uncertainty (at/g/yr) [d]	Muogenic ^{26}Al production rate at SLHL (*Sa*-scaled) (at/g/yr) [e]	2σ uncertainty (at/g/yr)	Total reference ^{26}Al production rate at SLHL (*Sa*-scaled) (at/g/yr)	2σ uncertainty (at/g/yr)
SPICE-A1	22.4	5.0	0.55	0.15	23.0	5.0	22.1	4.9	0.54	0.15	22.7	4.9
SPICE-A2	22.3	4.9	0.56	0.15	22.9	4.9	22.0	4.9	0.55	0.15	22.6	4.9
SPICE-A3	22.8	5.2	0.55	0.15	23.4	5.2	22.6	5.1	0.55	0.15	23.1	5.1
SPICE-A4	23.2	5.5	0.55	0.15	23.7	5.5	22.9	5.4	0.55	0.15	23.4	5.4
SPICE-A5	22.3	5.2	0.55	0.15	22.9	5.2	22.0	5.1	0.55	0.15	22.6	5.1
SPICE-A6	24.9	6.5	0.56	0.15	25.5	6.5	24.6	6.5	0.55	0.15	25.1	6.5
SPICE-A7	21.8	7.7	0.55	0.15	22.4	7.7	21.5	7.6	0.55	0.15	22.1	7.6
SPICE-A8	23.6	6.3	0.56	0.15	24.2	6.3	23.3	6.2	0.55	0.15	23.9	6.2
SPICE-A9	23.2	6.3	0.55	0.15	23.7	6.3	22.9	6.2	0.54	0.15	23.4	6.2
SPICE-A10	23.5	6.8	0.56	0.15	24.1	6.8	23.2	6.7	0.55	0.15	23.8	6.7
Average [f]	**22.9**	**2.2** ($2\sigma_{\bar{x}}$)	**0.56**	**0.06** ($2\sigma_{\bar{x}}$)	**23.5**	**2.2** ($2\sigma_{\bar{x}}$)	**22.6**	**2.2** ($2\sigma_{\bar{x}}$)	**0.55**	**0.06** ($2\sigma_{\bar{x}}$)	**23.2**	**2.2** ($2\sigma_{\bar{x}}$)

463 Note: $2\sigma_{\bar{x}}$ represents 2 standard errors associated with error-weighted means.

464 [a] Total concentrations of ^{26}Al are corrected for total shielding. Uncertainties include the uncertainties in nuclide concentration measurements and uncertainty related
465 to total shielding.

466 [b] Local production rates are calculated by using Equation (1) with t = 72 ka and $\lambda = 9.83\times10^{-7}$ yr^{-1}, corresponding to a ^{26}Al half-life of 705 kyr (Nishiizumi, 2004).
467 Uncertainties do not include the uncertainty on the ^{40}Ar/^{39}Ar age.

468 [c] Production of ^{26}Al from negative muon capture corrected for sample thickness and scaled for elevation, according to Heisinger et al. (2002a) and Lal (1991)/Stone
469 (2000), respectively; muogenic contributions to production rates determined here are independent of the calibration sample measurements, and only rely on
470 literature values. Scaling factors are listed in Table SD6. Uncertainty includes 9% and 12% relative uncertainties on the production rates from negative muon
471 capture and on scaling factors for negative muon capture (Heisinger et al., 2002a; 2002b).

472 [d] Uncertainty includes the uncertainty related to negative muon capture (column 7), as well as 14% relative uncertainty on production rates from fast muon induced
473 spallation (Heisinger et al., 2002a; 2002b) and uncertainty associated with total cosmogenic ^{26}Al concentrations (column 3).

474 [e] SLHL production rates are derived by scaling them to sea-level, high latitude using *St*, *Sf* and *Sa* scaling factors (Table SD6). The scaling factors are determined
475 using CRONUSCalc (Marrero et al., 2016) and the Matlab mmc1 code of Lifton et al. (2014). Uncertainties do not include the uncertainty on the ^{40}Ar/^{39}Ar age.

476 [f] This is an error-weighted mean of all ten samples. The $2\sigma_{\bar{x}}$ is the standard error on the mean and includes the uncertainty on the ^{40}Ar/^{39}Ar age.

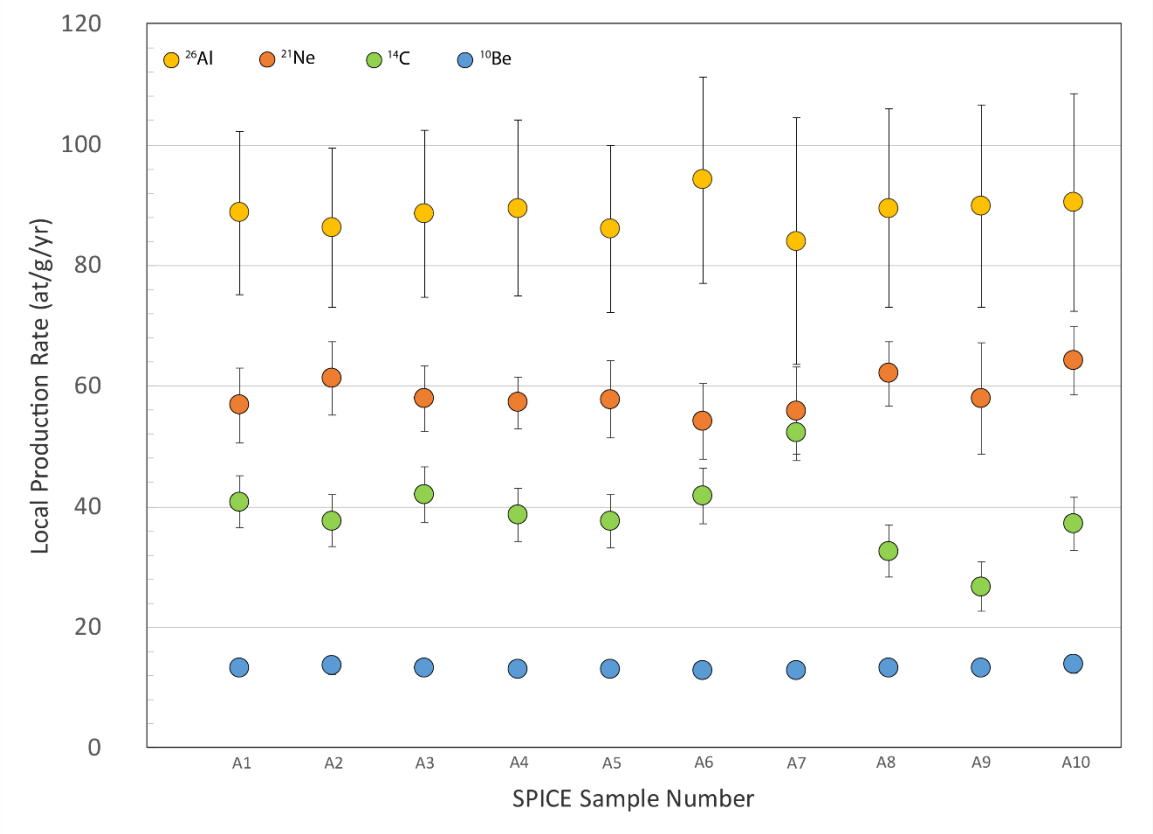

Figure 5. Local ^{26}Al, ^{21}Ne, ^{10}Be, and ^{14}C production rates for samples SPICE-A1 to –A10. These rates are not scaled to SLHL. Error bars represent 2σ uncertainty, and do not include the uncertainty associated with the ^{40}Ar/^{39}Ar age of the SP lava flow or the ^{14}C half-life. Cosmogenic ^{21}Ne, ^{10}Be, and ^{14}C production rates are from Fenton et al. (2019). Cosmogenic ^{14}C data from samples SPICE-A7 and -A9 are reported here for completeness, but are considered outliers (Fenton et al., 2019).

for ^{26}Al calculations in the online calculator of Balco et al. (2008), thus they are not listed in tables in this paper.

Time-dependent *Sf* and *Sa* scaling factors are integrated over 72 ka for ^{26}Al production rates (Table SD6). Likewise, those scaling factors were integrated over 72 ka for ^{21}Ne and ^{10}Be production rates, and over 25 ka for ^{14}C production rates (Fenton et al., 2019).

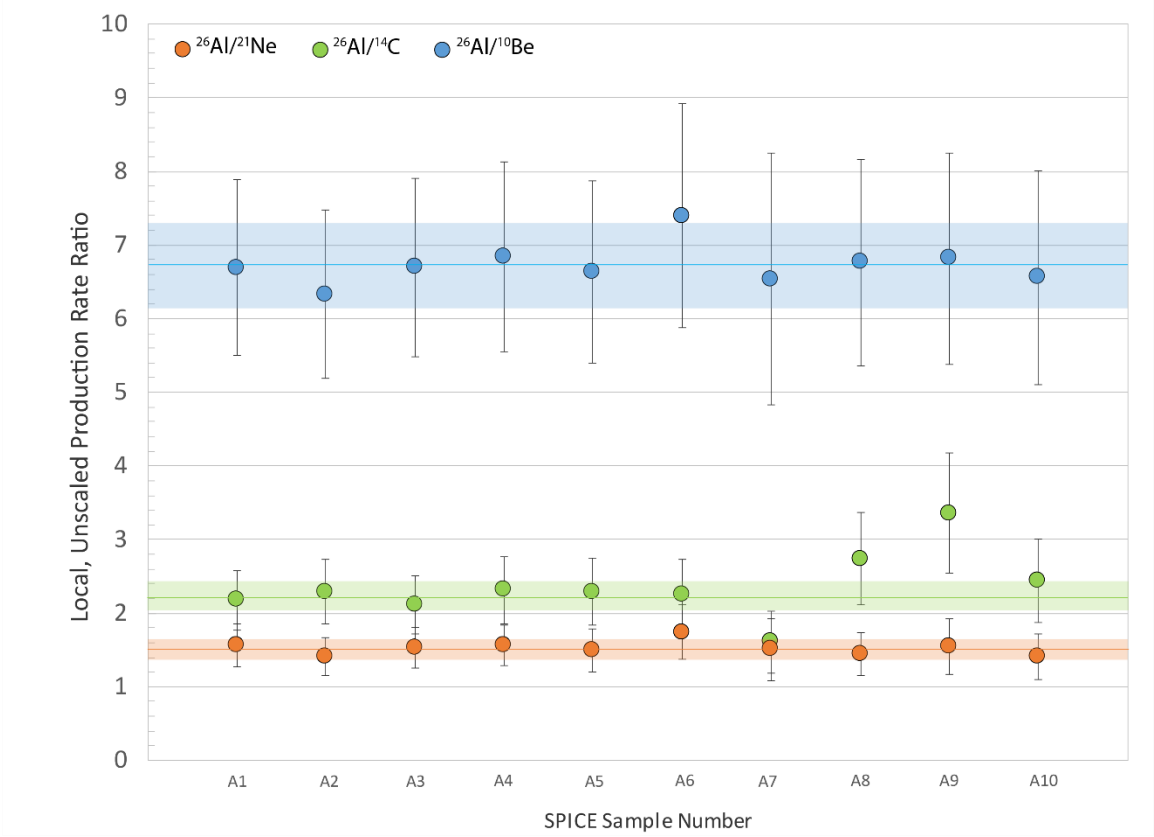

Figure 6. Local, unscaled production-rate ratios using cosmogenic ^{26}Al from this paper, and cosmogenic ^{21}Ne, ^{10}Be, and ^{14}C data originally published in Fenton et al. (2019). ^{26}Al/^{14}C ratios for samples SPICE-A7 and –A9 are shown here for completeness, but are considered outliers based on the ^{14}C data (Fenton et al., 2019). Shaded rectangles represent 2σ uncertainty of each error-weighted mean.

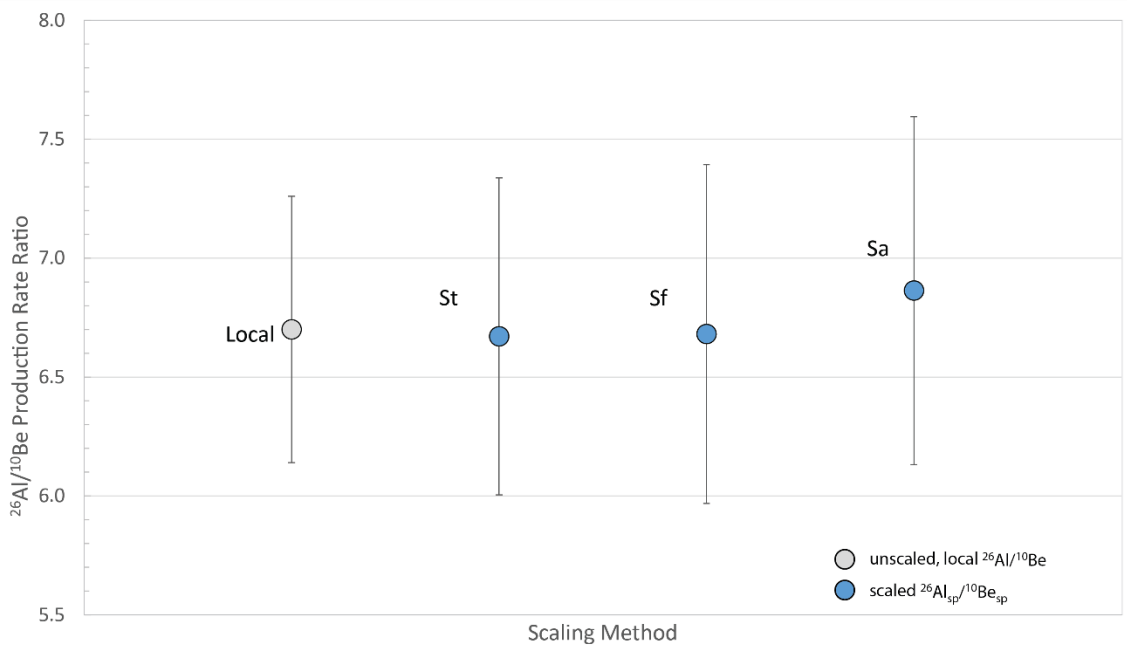

Figure 7. Error-weighted mean $^{26}Al/^{10}Be$ production ratios (2σ) for SPICE quartz samples. The gray circle indicates the ratio based on unscaled, local ^{26}Al and ^{10}Be production rates. The blue circles represent ratios of spallogenic $^{26}Al_{sp}/^{10}Be_{sp}$, scaled with *St*-, *Sf*-, and *Sa*-scaling methods.

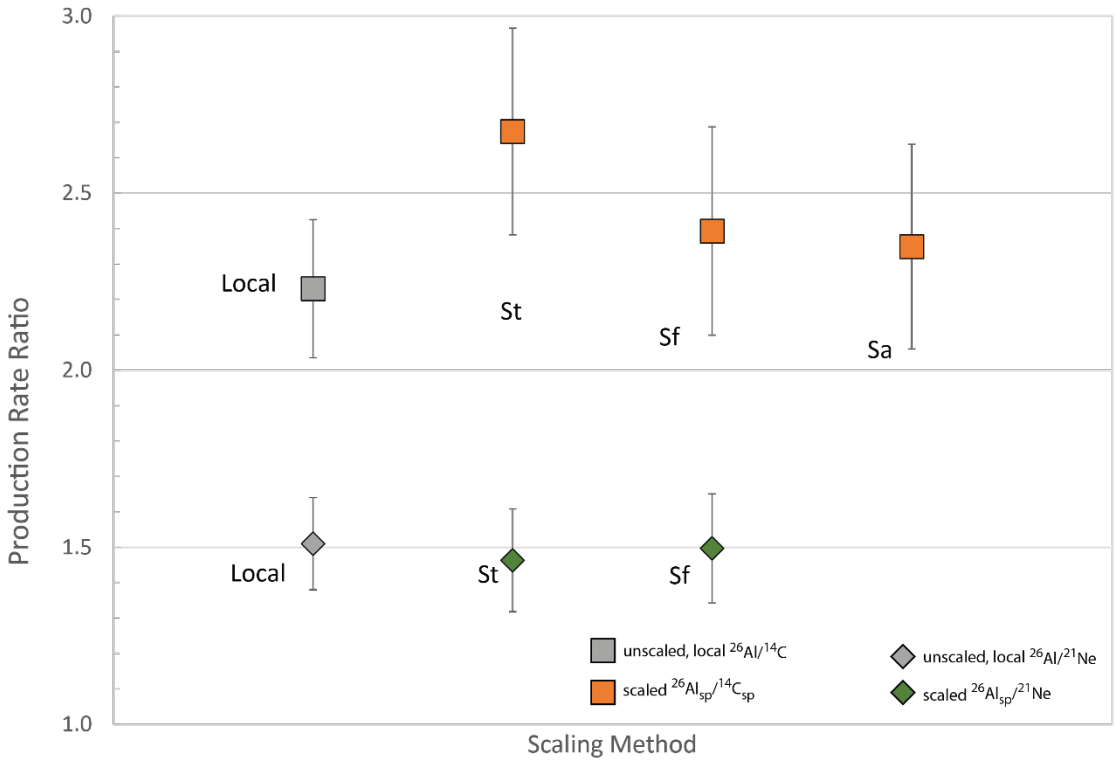

Figure 8. Error-weighted mean $^{26}Al/^{14}C$ (squares) and $^{26}Al/^{21}Ne$ (diamonds) values (2σ) for SPICE quartz samples. The gray symbols indicate ratios based on unscaled, local ^{26}Al, ^{14}C, and ^{21}Ne production rates. The colored symbols represent ratios of spallogenic $^{26}Al_{sp}/^{14}C_{sp}$ and $^{26}Al_{sp}/^{21}Ne$ scaled with *St*-, *Sf*-, and *Sa*-scaling methods.

6.3.1 Total reference SLHL production rates

Total reference SLHL production rates sum spallogenic and muogenic contributions to production rates for cosmogenic ^{26}Al (see footnotes to Table 5). Using time-independent *St* scaling factors yields error-weighted mean total reference SLHL production rates for cosmogenic ^{26}Al of 25.8 ± 2.5 at/g/yr. This rate agrees within uncertainty with the total reference SLHL cosmogenic ^{26}Al production rate of Luna et al. (2018; 27.1 ± 1.6 at/g/yr; 2σ), as derived using their ^{10}Be results in combination with the $^{26}Al/^{10}Be$ ratio given in Borchers et al. (2016). Using the time-dependent *Sf* and *Sa*

scaling methods, the SLHL ^{26}Al production rate in SPICE quartz decreases to 23.5 ± 2.2 at/g/yr and 23.2 ± 2.2 at/g/yr, respectively (Table 5). The three production rate values for *St*, *Sf*, and *Sa* scaling models agree within 2σ uncertainty.

6.3.2 SLHL production rates from muons and spallation

Muogenic contributions to ^{26}Al production rates at SPICE sample sites include production from both fast and slow muons and are calculated using the methods described and discussed in Heisinger et al. (2002a; 2002b). Production rates of muogenic ^{26}Al determined here are independent of SPICE calibration sample measurements and rely only on literature values in Heisinger et al. (2002a; 2002b).

Spallation production rates of ^{26}Al are derived by (1) subtracting the scaled production rates resulting from negative muon capture and fast-muon induced spallation from the local, unscaled reference ^{26}Al production rate at the corresponding sample elevation for each sample, and then (2) scaling the resultant spallogenic ^{26}Al production rates to SLHL using the scaling factors for neutron spallation. The spallation production rate includes the production from fast-muon induced spallation following Lal (1991)/Stone (2000) and Dunai(2000). Production rates by negative muons for ^{26}Al are listed in Table 5. *St*, *Sf,* and *Sa* scaling factors give muogenic ^{26}Al SLHL production rates of 0.80, 0.56, and 0.55 at/g/yr, respectively.

Spallogenic ^{26}Al contributes ~98% to total reference ^{26}Al production rates (Kober et al., 2011), in the absence of erosion. Time-independent *St* scaling factors yield an error-weighted mean spallation (*sp*) SLHL production rate for $^{26}Al_{sp}$ of 25.0 ± 2.4 at/g/yr (Table 5, Figure 9). Using the time-dependent *Sf* and *Sa* scaling methods, these SLHL values are 22.9 ± 2.2 at/g/yr and 22.6 ± 2.2 at/g/yr, respectively. The *Sf* and *Sa* scaling

548 methods result in an overall shift of data points in a graph similar to that in Figure 9, but
549 the individual positions of data points relative to one another do not change. All error-
550 weighted mean SLHL spallogenic ^{26}Al production rate values in SPICE quartz scaled
551 with the *St*, *Sf*, and *Sa* scaling methods agree within 2σ uncertainty (Table 5; Figures 9
552 and 10).

553 *St*-scaled and *Lm*-scaled spallation production rates for $^{26}Al_{sp}$ can also be calculated in
554 the online calculator of Balco et al. (2008;
555 https://hess.ess.washington.edu/math/v3/v3_cal_in.html). The calculator does not output
556 total reference ^{26}Al production rates. It yields indistinguishable, mean *St*-scaled and *Lm*-
557 scaled spallation SLHL production rates of 25.2 ± 2.2 at/g/yr and and 24.4 ± 2.2 at/g/yr,
558 respectively ($2\sigma_{SD}$; two standard deviations) for cosmogenic ^{26}Al in SPICE quartz (Table
559 3; Figure 2).

560
561 **7. Discussion**

562 All error-weighted mean SLHL spallogenic ^{26}Al production rate values in SPICE
563 quartz scaled with the *St*, *Sf*, and *Sa* scaling methods agree within 2σ uncertainty (Table
564 2; Figure 11). The SPICE project's error-weighted mean *St*-scaled SLHL spallogenic
565 $^{26}Al_{sp}$ production rate is 11% lower than the *St* scaled $^{26}Al_{sp}$ production rate of Borchers
566 et al. (2016), but would likely still overlap within 2σ uncertainty (Table 2; Figure 10) if it
567 had been reported with the Borchers et al. (2016) data. For example, if an uncertainty
568 were applied to the rates of Borchers et al. (2016) similar in magnitude to the uncertainty
569 calculated for the ^{26}Al production rates in this study (8 – 10 % $2\sigma_{SD}$ and $2\sigma_{\bar{x}}$; Table 2),
570 then the SPICE ^{26}Al production rates would clearly overlap those of Borchers et al.
571 (2016) (Table 2; Figure 10).

There are distinct differences between SPICE SLHL spallogenic $^{26}Al_{sp}$ production rates and the global average SLHL $^{26}Al_{sp}$ production rates of Borchers et al. (2016) scaled with the *Sf* and *Sa* scaling methods (Table 2). There is very little variation between the SLHL $^{26}Al_{sp}$ production rate values of Borchers et al. (2016; 27.9 – 28.6 at/g/yr) when scaled with the *St*, *Sf*, and *Sa* scaling methods. In contrast, SPICE SLHL $^{26}Al_{sp}$ production rate values show a decrease from 25.0 to 22.6 at/g/yr with use of time-dependent scaling methods, though the SPICE values do overlap within 2σ uncertainty (Figure 10).

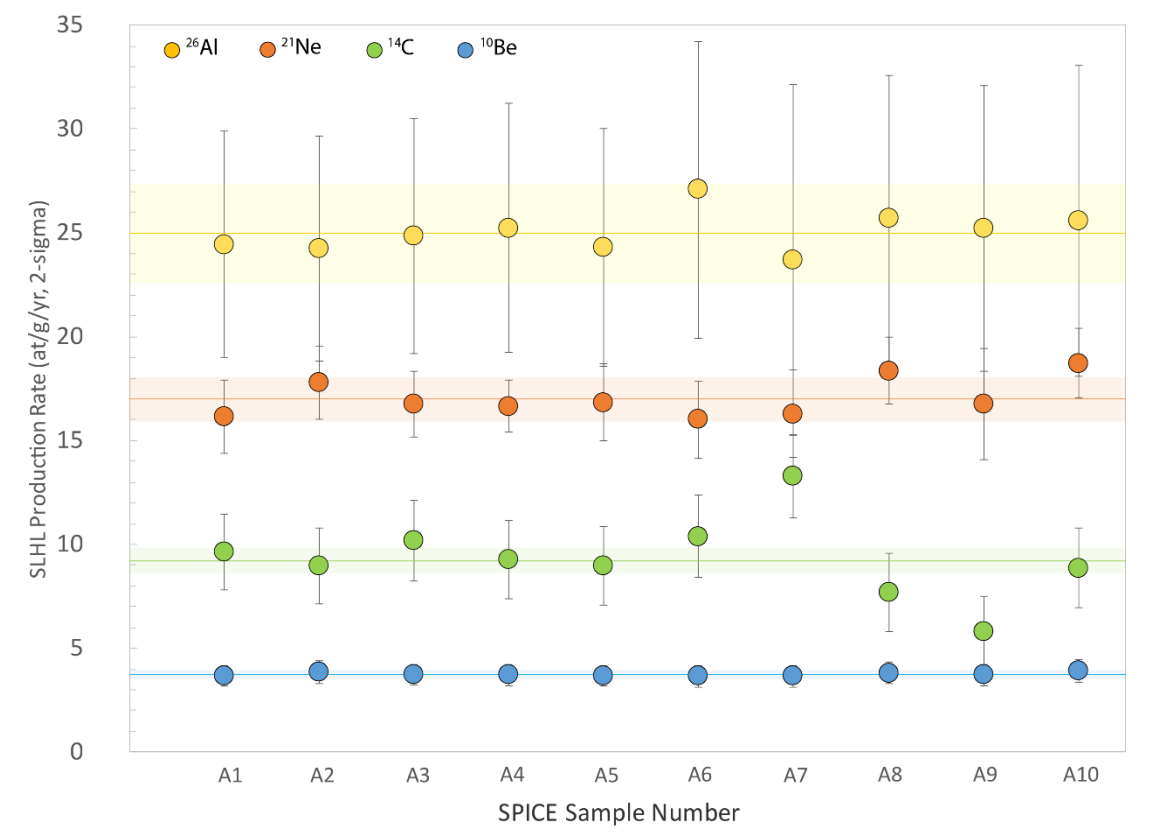

Figure 9. Total reference SLHL production rates for ^{21}Ne and spallation (*sp*) SLHL production rates for ^{26}Al, ^{10}Be and ^{14}C for samples SPICE-A1 to –A10. Rates are scaled with the *St* scaling method. Solid lines represent the error-weighted mean production rates for each nuclide. Production rates of ^{21}Ne, ^{10}Be, and ^{14}C are originally reported in Fenton et al. (2019). Shaded rectangles represent 2σ uncertainty of each error-weighted mean, and include the uncertainty associated with the $^{40}Ar/^{39}Ar$ age of the SP lava flow or

587 the radiocarbon half-life. Error bars on the circles represent 2σ uncertainty, and do not
588 include the uncertainty of the $^{40}Ar/^{39}Ar$ age.
589

590 The time periods over which *Sf* and *Sa* scaling factors are averaged have different
591 effects on the scaled ^{26}Al production rate values of Borchers et al (2016) and those of the
592 SPICE study. The $^{26}Al_{sp}$ production rates included in the Borchers et al. (2016) value are
593 from PPT, SCOT, and PERU sample sites with independent ages less than 20 ka. Time-
594 independent (*St*) and time-dependent (*Sf* and *Sa*) scaling methods produce very similar
595 scaling factors for these sites, and thus, the sites yield very similar production rate values
596 regardless of scaling model. The SP lava flow surface has been exposed to cosmic rays
597 for the past 72 ka, which includes a period of higher cosmic-ray flux between 20 and 50
598 ka, when the Earth's magnetic field was weaker than it is at present (Lifton et al., 2014).
599 Geomagnetic corrections are incorporated into *Sf* and *Sa* scaling factors.
600 Time-dependent *Sf* and *Sa* scaling factors are significantly greater than *St* scaling
601 factors at SPICE sample sites. Fenton et al. (2019) showed that *Sf* and *Sa* scaling factors
602 calculated for ^{10}Be at the SPICE-A1 site are 3.86 and 4.02, respectively, when averaged
603 over the past 72 ka, but are 9% and 16% lower (3.50 and 3.36, respectively) if averaged
604 over only the past 20 ka. Lower scaling factors yield higher SLHL cosmogenic nuclide
605 production rates. Fenton et al. (2019) also demonstrated that the 20-ka-averaged *Sf* and
606 *Sa* factors are only 0.5% lower and 3.4% higher than the constant *St* factor (3.52) at the
607 SPICE-A1 site, whereas the 72-ka-averaged *Sf* and *Sa* factors are 9.9% and 14.4% higher
608 than the *St* factor. This is because the *Sf* and *Sa* factors account for the weak geomagnetic
609 field between 20 and 50 ka (Lifton et al., 2014). These same corrections are included in
610 the *Sf* and *Sa* scaling factors for cosmogenic ^{26}Al (Table SD6) in SPICE quartz. *St* and *Sf*

611 scaling factors for cosmogenic ^{10}Be and ^{26}Al at SPICE sample sites are the same. All 72-
612 ka-averaged *Sf* and *Sa* factors for cosmogenic ^{26}Al at SPICE sample sites are 10% and
613 11% higher than the *St* factors at the same sites, respectively. *Sa* scaling factors for
614 cosmogenic ^{10}Be at SPICE sample sites (Fenton et al., 2019) are 3% higher than *Sa*
615 scaling factors for cosmogenic ^{26}Al at the same sites.

616 Fenton et al. (2019) demonstrated that there is no measurable difference between the
617 time independent, *St*-scaled production rates and time dependent, *Sf*- and *Sa*-scaled
618 production rates of cosmogenic ^{21}Ne and ^{10}Be in quartz at the SP flow over the past 72
619 ka. Fenton et al. (2019) concluded that either (1) production rates of ^{21}Ne and ^{10}Be in
620 quartz were not significantly greater during the proposed period of decreased magnetic
621 field strength from 20 to 50 ka, and/or (2) increased nuclide production during this period
622 is not recorded in SP flow quartz at a concentration that is detectable with current
623 precision and technology of AMS and noble gas mass spectrometry. SLHL production
624 rates of spallogenic ^{26}Al in SPICE quartz from this study also confirm that production
625 rates of ^{26}Al in SP flow quartz were not significantly greater between 20 and 50 ka,
626 and/or it is not yet possible to detect any increased cosmogenic nuclide production
627 (Figures 2 and 10).

628 Using the Balco et al. (2008) calculator, mean *St*-scaled and *Lm*-scaled SLHL $^{26}Al_{sp}$
629 production rates were calculated for SPICE quartz and for quartz in samples from the
630 PPT, SCOT, and PERU primary calibration sites of Borchers et al. (2016; data as given in
631 the ICE-D Production Rate Calibration Data database). The resultant mean *St* and *Lm*-
632 scaled SLHL $^{26}Al_{sp}$ production rates in SPICE quartz are 25.2 ± 2.2 and 24.4 ± 2.2
633 at/g/yr, respectively ($2\sigma_{SD}$; Table 3). This *St*-scaled spallation production rate is in

634 excellent agreement with the *St*-scaled spallation production rate calculated in this study
635 as an arithmetical mean outside of the Balco calculator (25.0 ± 1.9 at/g/yr; $2\sigma_{SD}$; Table 2;
636 Figure 2). The *Lm*-scaled mean SLHL spallogenic $^{26}Al_{sp}$ production rate in SPICE quartz
637 also agrees with *St*, *Sf*, and *Sa*-scaled rates in SPICE quartz within uncertainty. The
638 global, average spallation production rates calculated from combined PPT, SCOT, and
639 PERU data in this study are 30.0 ± 6.0 at/g/yr (*St*) and 30.5 ± 5.6 at/g/yr (*Lm*) ($2\sigma_{SD}$;
640 Table 3). These values are nominally higher than the *St* value reported in Borchers et al.
641 (2016; 27.9 at/g/yr), but all *St* and *Lm*-scaled rates from the PPT, SCOT, and PERU sites
642 still overlap within uncertainty. Online documentation for the calculator (Balco, 2017)
643 states "that the best-fitting reference production rates for *St* and *Lm* scaling are also not
644 comparable to similar values generated by other code." This indicates there is expected to
645 be a small degree of variation amongst production-rate values determined by various
646 online calculators and by individual computations, such as those seen in this study
647 (Tables 2 and 3; Figure 2). Mean *St*-scaled SLHL $^{26}Al_{sp}$ production rates in SPICE quartz
648 agree well with mean *St*-scaled SLHL $^{26}Al_{sp}$ production rates in quartz from PPT, SCOT,
649 and PERU calibration sites. The arithmetical mean *St*-scaled SLHL $^{26}Al_{sp}$ production
650 rates in both SPICE quartz (25.2 ± 2.2 at/g/yr; $2\sigma_{SD}$) and in quartz from the PPT, SCOT,
651 and PERU sites (26.5 ± 2.6 to 31.7 ± 4.4 at/g/yr, respectively; $2\sigma_{SD}$) overlap within
652 uncertainty (Figure 2). The *Lm*-scaled SPICE $^{26}Al_{sp}$ production rate overlaps the
653 arithmetical mean *Lm*-scaled SLHL $^{26}Al_{sp}$ production rates in quartz from the PPT and
654 PERU sites located in Utah (USA) and Peru, respectively; however, the arithmetical
655 mean *Lm*-scaled SLHL $^{26}Al_{sp}$ production rate (31.7 ± 4.4 at/g/yr; $2\sigma_{SD}$) in SCOT quartz
656 (Scotland) is higher than the arithmetical mean *Lm*-scaled SLHL $^{26}Al_{sp}$ production rate in

SPICE quartz (24.4 ± 2.2 at/g/yr; $2\sigma_{SD}$). The rates do not overlap within $2\sigma_{SD}$ uncertainty. *Lm* scaling includes time-dependent geomagnetic corrections, whereas *St* scaling does not.

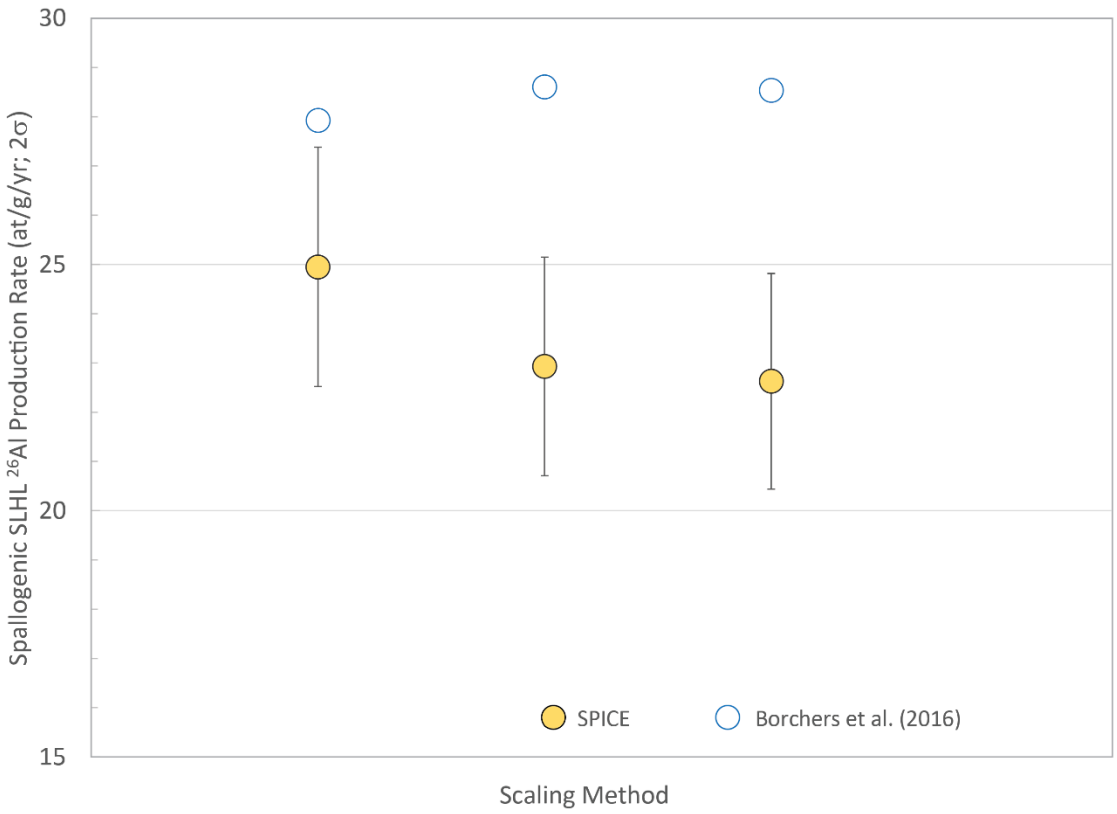

Figure 10. Error-weighted mean spallogenic ^{26}Al production rates (±2σ) in SPICE quartz (yellow circles) compared to calibrated spallogenic ^{26}Al production rates of Borchers et al. (2016) (white circles) scaled with *St*-, *Sf*-, and *Sa*-scaling methods.

665 Disagreement in SLHL $^{26}Al_{sp}$ production rates between the SPICE site (Arizona,
666 USA) and the SCOT site (Scotland) may indicate a quantifiable difference in $^{26}Al_{sp}$
667 production rate values that result from differences in latitude (~36°N vs ~57°N) and/or
668 elevation (1700 m vs 100-500 m) at the study sites as suggested by the scaling models of
669 Lifton et al. (2014) and Argento et al. (2015a; 2015b). These studies suggest that
670 production of individual cosmogenic nuclides in rock surfaces might increase at different
671 rates as latitude and altitude increase. A study in Greenland (~60 - 76°N and 50 – 620 m
672 elevation; Corbett et al., 2017) recently indicated that the $^{26}Al/^{10}Be$ production-rate ratio
673 in quartz is higher (7.3 ± 0.6; 2σ) in the Arctic than the canonical, 'global' $^{26}Al/^{10}Be$
674 value of 6.75. The higher $^{26}Al/^{10}Be$ production-rate ratio of Corbett et al. (2017) might
675 indicate increased $^{26}Al_{sp}$ production rates at high latitudes (> 60°N), compared to $^{26}Al_{sp}$
676 production rates at mid-latitude SPICE sites (~36°N, 112°W, Arizona, USA) and PPT
677 sites (~41°N, 112°W, Utah, USA). The SCOT site, located in Scotland at ~57°N, has a
678 SLHL $^{26}Al_{sp}$ production rate of 31.7 ± 4.4 at/g/yr (2σ; *Lm*). SPICE quartz and PPT
679 quartz yield SLHL $^{26}Al_{sp}$ production rates of 24.4 ± 2.2 (2σ; *Lm*) and 28.2 ± 6.0 at/g/yr
680 (2σ; *Lm*), respectively. Note that the SPICE and PPT sites are at roughly the same
681 longitude, but the PPT site is ~5°N of the SPICE locale. It is also worth noting, the higher
682 $^{26}Al/^{10}Be$ production-rate ratio of Corbett et al. (2017) might instead be related to a
683 higher erosion rate and/or possible burial of samples that could result in greater muogenic
684 contributions to production of ^{26}Al and ^{10}Be and thus a higher production rate ratio at
685 their sites.
686 Significant burial and erosion of a landform surface decreases cosmogenic nuclide
687 concentrations at that surface. Field evidence indicates negligible erosion of the surfaces

688 of SPICE sample sites (section 4 and photographs of sample sites in Supplemental Data
689 of Fenton et al., 2019). If SPICE samples were affected by significant erosion and/or
690 burial, reduced production of cosmogenic ^{26}Al would be recorded in quartz samples and
691 rates would not agree so well with other ^{26}Al rates in the literature (Figures 2, 3, and 10).
692 Calculations based on ^{26}Al in this study indicate erosion rates of 1.25 – 3.0 mm/kyr
693 would be required to compensate for the small difference in the *St*-scaled SLHL ^{26}Al
694 production rates of eight SP flow surface samples and the *St* scaled SLHL ^{26}Al
695 production rate reported by Borchers et al. (2016; 27.9 at/g/yr; Table 2). The remaining
696 two SP flow samples would require a much lower erosion rate of 0.03 mm/kyr. The
697 higher calculated erosion rates are generally in agreement with erosion rates (0.2 – 1.9
698 mm/kyr) calculated by Fenton et al. (2019) based on differences between SLHL
699 production rates of ^{21}Ne and ^{10}Be in SPICE quartz and SLHL ^{21}Ne and ^{10}Be production
700 rates reported by Borchers et al. (2016). Fenton et al. (2019), however, present a strong
701 argument that the available field evidence simply does not support this magnitude of
702 surface denudation (9 – 22 cm), nor the magnitude (10^1 – 10^2 cm) required to account for
703 differences in SPICE production rates of cosmogenic ^{21}Ne, ^{14}C, and ^{10}Be and those of
704 Borchers et al. (2016; see section 4).

705 SPICE SLHL spallogenic $^{26}Al_{sp}$ production rates scaled with the *St*, *Sf*, and *Lm*
706 scaling methods agree within uncertainty with the modeled SLHL spallogenic ^{26}Al
707 production rate of 29.6 ± 4.4 at/g/yr of Argento et al. (2015a) (Tables 2, 3, and 4). The
708 *Sa*-scaled SPICE SLHL spallogenic $^{26}Al_{sp}$ production rate (22.6 ± 2.2 at/g/yr; $2\sigma_{\bar{x}}$) is
709 lower than and does not overlap within uncertainty the rate of Argento et al. (2015a).

710 This is likely due to differences in calculations between the scaling models of Argento et
711 al. (2015a; 2015b) and Lifton et al. (2014).
712 SP flow quartz has mean $^{26}Al/^{10}Be$ values that agree very well with previously
713 published, calibrated and modeled production-rate ratios within $2\sigma_{SD}$ uncertainty (see
714 section 3; Tables 4, SD1, SD2, SD3, and SD5; Figures 3, 11, and 12). Local production-
715 rate $^{26}Al/^{10}Be$ values for SPICE, PPT, SCOT, and PERU primary calibration sites are 6.7
716 ± 0.6, 6.53 ± 0.14, 7.19 ± 0.18, and 6.74 ± 0.34, respectively. Ratios based on SLHL
717 spallogenic production rates of cosmogenic ^{26}Al and ^{10}Be from the SPICE study,
718 Borchers et al. (2016) and Argento et al. (2015a) agree well with each other regardless of
719 scaling method. Uncertainties are not reported with the Borchers et al. (2016) data, thus,
720 no uncertainties are reported with the associated ratios below. The $^{26}Al_{sp}/^{10}Be_{sp}$ values in
721 quartz for SPICE, Borchers et al. (2016), and Argento et al. (2015a) are 6.7 ± 0.7 (*St*),
722 6.97 (*St*), and 6.7 ± 1.4, respectively (Tables 4, SD3, and SD5; Figures 11 and 12). When
723 scaled with the *Sf* scaling model, the $^{26}Al_{sp}/^{10}Be_{sp}$ values for SPICE and Borchers et al.
724 (2016) are 6.7 ± 0.7 and 7.00, respectively. $^{26}Al_{sp}/^{10}Be_{sp}$ values for SPICE and Borchers
725 et al. (2016) are 6.9 ± 0.7 and 7.28, respectively, when scaled with the *Sa* scaling method.
726 Likewise, the *Lm*-scaled $^{26}Al_{sp}/^{10}Be_{sp}$ value (6.8 ± 0.7) for SPICE quartz overlaps the *Lm*-
727 scaled $^{26}Al_{sp}/^{10}Be_{sp}$ value (6.98) of Borchers et al. (2016) within uncertainty.
728 SP flow quartz also has mean $^{26}Al/^{14}C$ ratios that agree well with previously
729 published, calibrated and modeled production-rate ratios within $2\sigma_{SD}$ uncertainty (Tables
730 4, SD2, SD3, and SD5; Figures 11 and 12). Data from Lifton et al. (2015) yield a local,
731 unscaled production-rate $^{26}Al/^{14}C$ of 1.90 ± 0.33 in Promontory Point (PPT) quartz
732 samples. This PPT $^{26}Al/^{14}C$ value overlaps the local, unscaled production-rate ratio of

733 2.23 ± 0.20 in SPICE quartz within uncertainty (Tables SD2 and SD5). Ratios based on
734 SLHL spallogenic production rates of cosmogenic ^{26}Al and ^{14}C from the SPICE project
735 (Fenton et al., 2019; this study) and from Argento et al. (2015a) agree within uncertainty.
736 The $^{26}Al_{sp}/^{14}C_{sp}$ values (*St*) for SPICE and Argento et al. (2015a) are 2.67 ± 0.29 and 1.96
737 ± 0.42, respectively (Tables 4, SD3 and SD5; Figure 12). The SPICE $^{26}Al_{sp}/^{14}C_{sp}$ value
738 (2.67 ± 0.29) would likely overlap the $^{26}Al_{sp}/^{14}C_{sp}$ value (2.28) of Borchers et al. (2016)
739 within uncertainty if it were reported for the latter value. When scaled with the *Sf* scaling
740 model, the $^{26}Al_{sp}/^{14}C_{sp}$ values for SPICE and Borchers et al. (2016) are 2.39 ± 0.29 and
741 2.25, respectively. $^{26}Al_{sp}/^{14}C_{sp}$ values for SPICE and Borchers et al. (2016) are 2.35 ±
742 0.29 and 2.24, respectively, when scaled with the *Sa* scaling method. The *Lm*-scaled
743 $^{26}Al_{sp}/^{14}C_{sp}$ value (2.5 ± 1.0) for SPICE quartz overlaps the *Lm*-scaled $^{26}Al_{sp}/^{14}C_{sp}$ value
744 (2.29) of Borchers et al. (2016). Thus, *Sf*, *Sa*, and *Lm*-scaled $^{26}Al_{sp}/^{14}C_{sp}$ values for SPICE
745 quartz overlap within uncertainty $^{26}Al_{sp}/^{14}C_{sp}$ values reported by both Borchers et al.
746 (2016) and Argento et al. (2015a) (Figures 11 and 12). It is important to note, while ratios
747 may agree within uncertainty, it does not mean that individual spallation production rates
748 reported in Argento et al (2015a) agree with spallation production rates reported in
749 Fenton et al. (2019). For example, the spallation production rates of neither ^{21}Ne nor ^{14}C
750 from Argento et al. (2015a) agree with those of Fenton et al. (2019) within uncertainty,
751 regardless of *St*, *Sf*, *Sa*, or *Lm* scaling method (Table 4; Figure 13); however, the
752 propagation of the uncertainty on the $^{26}Al_{sp}$ production rate of Argento et al. (2015a;
753 15%) through calculation of the $^{26}Al_{sp}/^{14}C_{sp}$ value results in a larger uncertainty (~20%)
754 that overlaps well with $^{26}Al_{sp}/^{14}C_{sp}$ values (Table 4).

There is somewhat less agreement between average $^{26}Al_{sp}/^{21}Ne$ values measured in SP flow quartz and previously published, calibrated and modeled production-rate $^{26}Al_{sp}/^{21}Ne$ values in the literature (Tables 4 and SD3; Figures 11, and 12). Goethals et al. (2009), Niedermann et al. (1994), and Balco and Shuster (2009) report calibrated $^{26}Al/^{21}Ne$ production ratios of 1.80 ± 0.09, 1.65 ± 0.28 and 1.65 ± 0.15, respectively, in quartz. The SPICE $^{26}Al_{sp}/^{21}Ne$ value (1.46 ± 0.14) agrees within uncertainty with the ratios of Niedermann et al. (1994) and Balco and Shuster (2009), however, the SPICE $^{26}Al/^{21}Ne$ does not agree within uncertainty with the $^{26}Al/^{21}Ne$ value of Goethals et al. (2009). This is likely due to the greater SLHL ^{26}Al production rate (36.2 at/g/yr) estimated from measurements in quartz from the surface of the Bishop Tuff (Goethals et al., 2009). The $^{26}Al_{sp}/^{21}Ne$ values for SPICE, Borchers et al. (2016), and Argento et al. (2015a) are 1.46 ± 0.14 (*St*), 1.68 (*St*), and 2.43 ± 0.51. While the $^{26}Al_{sp}/^{21}Ne$ values from SPICE quartz agree with $^{26}Al_{sp}/^{21}Ne$ values calculated from data in Borchers et al. (2016) within $2\sigma_{SD}$ uncertainty (Figure 11), the mean *St*, *Lm* and *Sf* SPICE $^{26}Al_{sp}/^{21}Ne$ values do not overlap the $^{26}Al_{sp}/^{21}Ne$ value of Argento et al. (2015a) within uncertainty (Figure 12). This is likely because the modeled SLHL ^{21}Ne production rate of Argento et al. (2015a; 12.2 ± 1.8 at/g/yr) is significantly less than the calibrated ^{21}Ne production rate in SP flow quartz (16.7 ± 2.1 at/g/yr (*St*); Fenton et al., 2019), resulting in a higher $^{26}Al_{sp}/^{21}Ne$ value. The *Sf*-scaled calibrated $^{26}Al_{sp}$ and ^{21}Ne production rates in SP flow quartz are 23.0 ± 1.8 and 15.3 ± 1.9 at/g/yr, respectively (Fenton et al., 2019). These rates yield a $^{26}Al_{sp}/^{21}Ne$ value (*Sf*) of 1.50 ± 0.15, which still does not agree within uncertainty with the $^{26}Al_{sp}/^{21}Ne$ value (2.43 ± 0.51) derived from the study of Argento et al. (2015a). There is no *Lm* or *Sa*-scaled $^{26}Al_{sp}/^{21}Ne$ value reported in Borchers et al. (2016). There is no *Sa*-

778 scaled $^{26}Al_{sp}/^{21}Ne$ value calculated for SPICE quartz (Table SD5), because the mmc1
779 code of Lifton et al. (2014) does not provide the possibility of calculating *Sa* scaling
780 factors for ^{21}Ne.
781

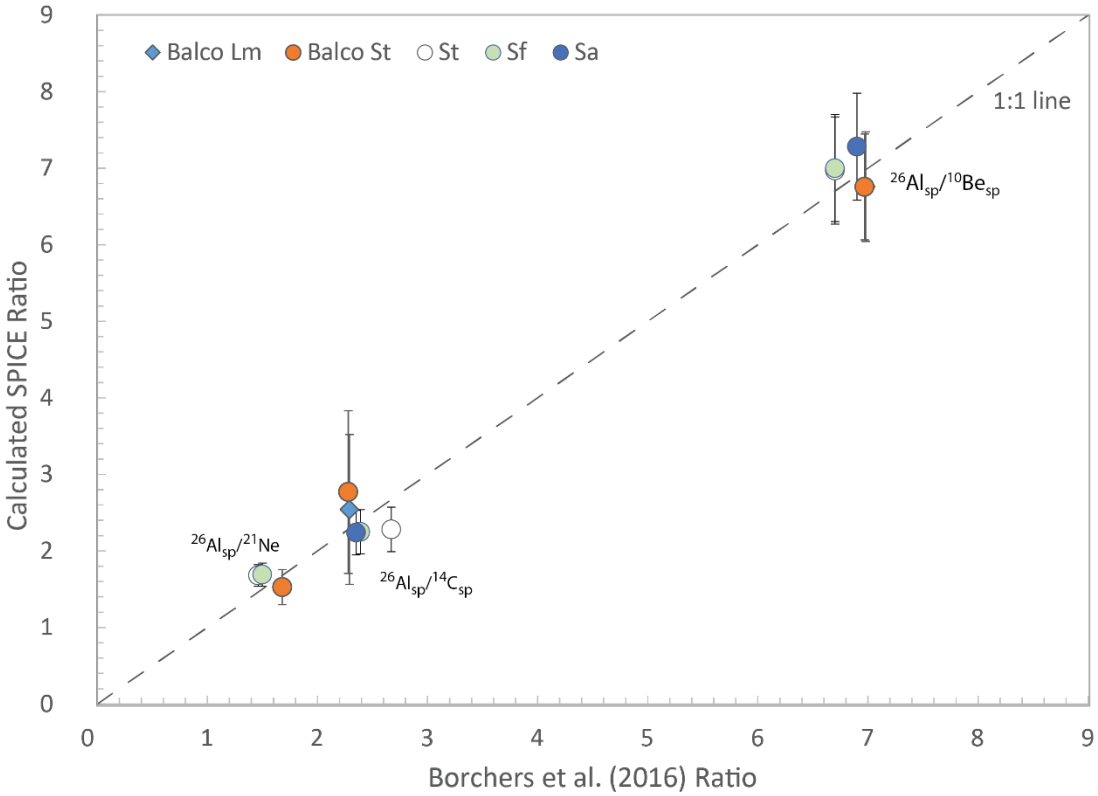

782

783 Figure 11. Comparison of production-rate ratios from the SPICE project (this study and
784 Fenton et al., 2019) and from Borchers et al. (2016) based on spallation production rates
785 of cosmogenic ^{26}Al, ^{21}Ne, ^{14}C, and ^{10}Be in quartz and *St*, *Sf*, *Sa*, and *Lm* scaling methods.
786 "Balco Lm" and "Balco St" indicate ratios based on data calculated in this study in the
787 online calculator of Balco et al. (2008).
788

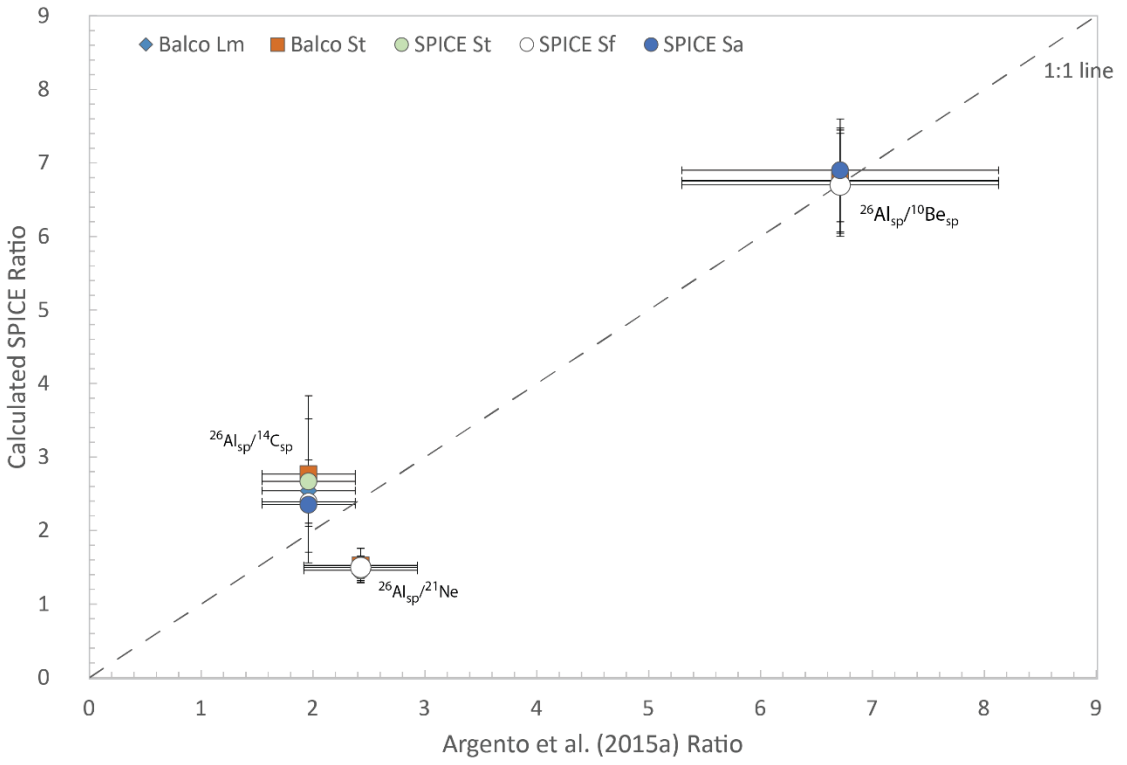

789

790 Figure 12. Comparison of production-rate ratios from the SPICE project (this study and
791 Fenton et al., 2019) and from Argento et al. (2015a) based on spallation production rates
792 of cosmogenic ^{26}Al, ^{21}Ne, ^{14}C, and ^{10}Be in quartz. SPICE samples were scaled using *St*,
793 *Sf*, *Sa*, and *Lm* scaling methods. "Balco Lm" and "Balco St" indicate ratios based on data
794 calculated in this study in the online calculator of Balco et al. (2008). Ratios based on
795 data from Argento et al. (2015a) are scaled based on their nuclear-physics based model.
796

797

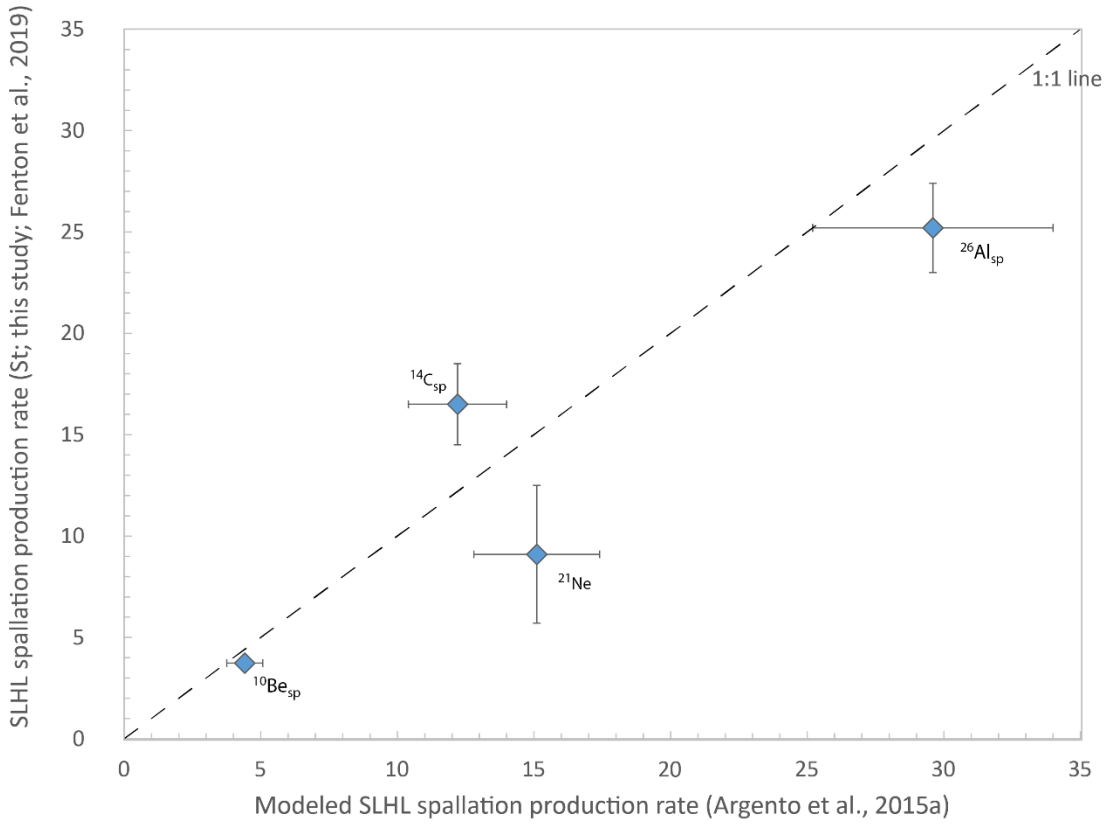

798

799 Figure 13. Comparison of SLHL spallation production rates from the SPICE study (this
800 study and Fenton et al., 2019) and from Argento et al. (2015a) based on spallation
801 production rates of cosmogenic ^{26}Al, ^{21}Ne, ^{14}C, and ^{10}Be in quartz. SPICE samples were
802 scaled using the *St* method. Production rates based on data from Argento et al. (2015a)
803 are scaled based on their nuclear-physics based model.
804

805
806 **8. Conclusions**

807 This second publication of the SPICE project adds production rates of cosmogenic
808 ^{26}Al to the robust dataset of cross-calibrated production rates of cosmogenic ^{21}Ne, ^{10}Be,
809 and ^{14}C in quartz from the SP lava flow. Cosmogenic ^{26}Al production rates are calibrated
810 to the independent ^{40}Ar/^{39}Ar age of the lava flow (72±4 ka; 2σ; Fenton et al., 2013).
811 Cosmogenic ^{26}Al production rate values for each SPICE quartz sample agree within 2σ
812 uncertainty.

Measurements of cosmogenic ^{26}Al in SP flow quartz yield an error-weighted mean SLHL total reference ^{26}Al production rate of 25.8 ± 2.5 at/g/yr (2σ; *St* scaling). This SPICE production rate agrees very well and within 2σ uncertainty with *St*-scaled SLHL total reference ^{26}Al and spallogenic ^{26}Al production rates reported in the literature (Lifton et al., 2015; Kelly et al., 2015; Borchers et al., 2016).

The *St*-scaled spallogenic ^{26}Al rate is 25.0 ± 2.4 at/g/yr integrated over the past 72 ka. This rate overlaps within 2σ uncertainty with other *St*-scaled production rate values in the literature. SLHL spallogenic ^{26}Al production rates are lower if time-dependent *Sf*, *Sa*, and *Lm* scaling factors are used, yielding values of 22.9 ± 2.2 at/g/yr, 22.6 ± 2.2 at/g/yr, and 24.4 ± 2.2 at/g/yr (2σ), respectively.

The error-weighted mean SLHL spallogenic ^{26}Al production rate of 25.0 ± 2.4 at/g/yr (2σ; *St* scaling) determined for SP flow quartz is nominally lower but would likely overlap the global, average $^{26}Al_{sp}$ production rate of Borchers et al. (2016; 27.9 at/g/yr (*St*)) within 2σ uncertainty if uncertainty were reported with the latter value. The spallogenic $^{26}Al_{sp}$ production rates calibrated in SPICE quartz using the online calculator of Balco et al. (2008) are 25.2 ± 2.2 and 24.4 ± 2.2 at/g/yr ($2\sigma_{SD}$; *St* and *Lm* scaling, respectively). These SPICE $^{26}Al_{sp}$ production rates are nominally lower, but agree with global, average $^{26}Al_{sp}$ production rates of Borchers et al. (2016) within 2σ uncertainty when rates are determined with the same calculator: 30.0 ± 6.0 and 30.5 ± 5.6 at/g/yr ($2\sigma_{SD}$; *St* and *Lm* scaling, respectively). This SPICE study shows there is variation in ^{26}Al production rates mainly due to numerical differences in various scaling methods, and thus scaling factors, but there is no measurable difference between the *St*-scaled production rates of cosmogenic ^{26}Al at the SP flow over the past 20 ka and rates over the past 72 ka.

836 This could mean that ^{26}Al production rates in quartz were not significantly greater during
837 the proposed period of decreased magnetic field strength from 20 to 50 ka. It could also
838 mean that increased nuclide production during this period is not recorded in SP flow
839 quartz at a level that is detectable with current precision and technology of AMS.
840 Preservation of the surface of the SP lava flow argues against any significant erosion.
841 The SPICE study suggests that the *St*-scaled production rates of cosmogenic ^{26}Al can
842 be used to calculate accurate exposure ages and erosion rates on surfaces between 20 and
843 70 ka in age. If future exposure studies calculate erosion rates and exposure ages using
844 the time-dependent *Sf*, *Sa,* or *Lm* scaling methods, particularly for landforms that are ~70
845 ka, then *Sf-, Sa-,* or *Lm*-scaled SLHL ^{26}Al production rates from the SPICE quartz study
846 should be used as reference SLHL rates for these calculations. Use of the time-dependent
847 *Sf* and *Sa* scaling methods in concert with the *Sf* and *Sa* SLHL $^{26}Al_{sp}$ production rates of
848 Borchers et al. (2016; 28.6 and 28.5 at/g/yr) could result in underestimated exposure ages
849 and interpretations of erosional and/or burial effects where none are present.
850 Comparison of ^{26}Al/^{10}Be, ^{26}Al/^{14}C, and ^{26}Al/^{21}Ne measured in SPICE quartz
851 generates both agreement and disagreement, within uncertainty, with previously
852 published, calibrated and modeled values in the literature. SP flow quartz has average
853 ^{26}Al/^{10}Be and ^{26}Al/^{14}C values that agree very well with previously published calibrated
854 and modeled production-rate ratios within uncertainty. SPICE ^{26}Al/^{21}Ne values agree
855 well with calibrated ^{26}Al/^{21}Ne values of Niedermann et al. (1994) and Balco and Shuster
856 (2009), however, the SPICE ^{26}Al/^{21}Ne does not agree within uncertainty with the
857 ^{26}Al/^{21}Ne value of Goethals et al. (2009). SPICE $^{26}Al_{sp}$/^{21}Ne values agree well with the
858 calibrated ^{26}Al/^{21}Ne values of Borchers et al. (2016), but there is no agreement between

calibrated SPICE $^{26}Al_{sp}/^{21}Ne$ values and the modeled $^{26}Al_{sp}/^{21}Ne$ values of Argento et al. (2015a).

Furthermore, SPICE $^{26}Al_{sp}/14C_{sp}$ values may agree within uncertainty with those modeled by Argento et al. (2015a), but that does not imply that individual, modeled spallation production rates reported in Argento et al (2015a) agree with spallation production rates reported in Fenton et al. (2019). Neither of the individual spallation production rates of ^{21}Ne and $^{14}C_{sp}$ from Argento et al. (2015a) agree with spallation production rates of ^{21}Ne and $^{14}C_{sp}$ of Fenton et al. (2019) within uncertainty, regardless of *St*, *Sf*, *Sa*, or *Lm* scaling method. Lastly, nominally lower SLHL production of $^{26}Al_{sp}$ at the SPICE site (Arizona, USA) compared to the SCOT site (Scotland) may indicate a quantifiable difference in $^{26}Al_{sp}$ production rate values that result from differences in latitude (~36°N vs ~57°N) and/or elevation (1700 m vs 100-500 m) (Lifton et al., 2014; Argento et al., 2015a; 2015b).

Acknowledgements

We gratefully acknowledge field, laboratory, and technical support from Hella Wittmann-Oelze, Marina Ospald, Hartmut Liep, Juliane Herwig, Johannes Glodny, Shasta Marrero and Simon Merrall. We also thank Régis Braucher, two anonymous reviewers, CRONUS-EU and CRONUS-Earth colleagues, and Lawrence S. Jones for very helpful critical discussions and reviews. This study was funded by the Deutsche Forschungsgemeinschaft (DFG Project Reference Number FE 1418/1-1) and by GFZ Potsdam.

References

Altmaier, M., Herpers, U., Delisle, G., Merchel, S., Ott, U., 2010. Glaciation history of Queen Maud Land (Antarctica) reconstructed from in-situ produced cosmogenic ^{10}Be, ^{26}Al and ^{21}Ne. Polar Sci. 4, 42–61. https://doi.org/10.1016/J.POLAR.2010.01.001

Anderson, R.S., Repka, J.L., Dick, G.S., 1996. Explicit treatment of inheritance in dating depositional surfaces using in situ ^{10}Be and ^{26}Al. Geology 24, 47–51.

Argento, D. C., Stone, J. O., Reedy, R. C., O'Brien, K., 2015a. Physics-based modeling of cosmogenic nuclides part I–radiation transport methods and new insights. Quat. Geochronol. 26, 29-43. http://dx.doi.org/10.1016/j.quageo.2014.09.004

Argento, D. C., Stone, J. O., Reedy, R. C., O'Brien, K., 2015b. Physics-based modeling of cosmogenic nuclides part II–key aspects of in-situ cosmogenic nuclide production. Quat. Geochronol. 26, 44-55. http://dx.doi.org/10.1016/j.quageo.2014.09.005

Baksi, A.K., 1974. K–Ar Study of the S.P. Flow. Can. J. Earth Sci. 11, 1350–1356. https://doi.org/10.1139/e74-131

Balco, G., 2017. Feb 23, Documentation -- V3 Exposure Age Calculator. Retrieved from https://sites.google.com/a/bgc.org/v3docs/home

Balco, G., Shuster, D.L., 2009. ^{26}Al –^{10}Be –^{21}Ne burial dating. Earth Planet. Sci. Lett. 286, 570–575. https://doi.org/10.1016/J.EPSL.2009.07.025

Balco, G., Stone, J.O., Lifton, N.A., Dunai, T.J., 2008. A complete and easily accessible means of calculating surface exposure ages or erosion rates from ^{10}Be and ^{26}Al measurements. Quat. Geochronol. 3, 174–195. https://doi.org/10.1016/J.QUAGEO.2007.12.001

Balco, G., Stone, J.O.H., Sliwinski, M.G., Todd, C., 2014. Features of the glacial history of the Transantarctic Mountains inferred from cosmogenic ^{26}Al, ^{10}Be and ^{21}Ne concentrations in bedrock surfaces. Antarct. Sci. 26, 708–723.

Bierman, P., Turner, J., 1995. ^{10}Be and ^{26}Al evidence for exceptionally low rates of Australian bedrock erosion and the likely existence of pre-Pleistocene landscapes. Quat. Res. 44, 378–382. https://doi.org/10.1006/QRES.1995.1082

Billingsley, G.H., Priest, S.S., Felger, T.J., 2007. Geologic Map of the Cameron 30′ X 60′ Quadrangle, Coconino County, Northern Arizona. Citeseer.

Binnie, S.A., Dunai, T.J., Voronina, E., Goral, T., Heinze, S., Dewald, A., 2015. Separation of Be and Al for AMS using single-step column chromatography. Nucl. Instruments Methods Phys. Res. Sect. B Beam Interact. with Mater. Atoms 361, 397–401. https://doi.org/10.1016/J.NIMB.2015.03.069

Binnie, S.A., Dewald, A., Heinze, S., Voronina, E., Hein, A., Wittmann, H., von Blanckenburg, F., Hetzel, R., Christl, M., Schaller, M., Léanni, L., ASTER Team, Hippe, K., Vockenhuber, C., Ivy-Ochs, S., Maden, C., Fülöp, R.-H., Fink, D., Wilcken, K.M., Fujioka, T., Fabel, D., Freeman, S.P.H.T., Xu, S., Fifield, L.K., Akçar, N., Spiegel, C., Dunai, T.J., 2019. Preliminary results of CoQtz-N: A quartz reference material for terrestrial in-situ cosmogenic ^{10}Be and ^{26}Al measurements. Nucl. Instruments Methods Phys. Res. Sect. B Beam Interact. with Mater. Atoms 456, 203–212. https://doi.org/10.1016/J.NIMB.2019.04.073

Blard, P.-H., Lupker, M., Rousseau, M., 2019. Paired-cosmogenic nuclide paleoaltimetry.

927 Earth Planet. Sci. Lett. 515, 271–282.
928 https://doi.org/https://doi.org/10.1016/j.epsl.2019.03.005
929 Borchers, B., Marrero, S., Balco, G., Caffee, M., Goehring, B., Lifton, N., Nishiizumi,
930 K., Phillips, F., Schaefer, J., Stone, J., 2016. Geological calibration of spallation
931 production rates in the CRONUS-Earth project. Quat. Geochronol. 31, 188–198.
932 https://doi.org/10.1016/J.QUAGEO.2015.01.009
933 Briner, J.P., Lifton, N.A., Miller, G.H., Refsnider, K., Anderson, R., Finkel, R., 2014.
934 Using in situ cosmogenic ^{10}Be, ^{14}C, and ^{26}Al to decipher the history of polythermal
935 ice sheets on Baffin Island, Arctic Canada. Quat. Geochronol. 19, 4–13.
936 https://doi.org/10.1016/J.QUAGEO.2012.11.005
937 Brook, E.J., Brown, E.T., Kurz, M.D., Ackert, R.P., Raisbeck, G.M., Yiou, F., 1995.
938 Constraints on age, erosion, and uplift of Neogene glacial deposits in the
939 Transantarctic Mountains determined from in situ cosmogenic ^{10}Be and ^{26}Al.
940 Geology 23, 1063–1066. https://doi.org/10.1130/0091-
941 7613(1995)023<1063:COAEAU>2.3.CO;2
942 Brook, E.J., Brown, E.T., Kurz, M.D., Raisbeck, G.M., Yiou, F., 1996. An Antarctic
943 perspective on in-situ cosmogenic nuclide production. Radiocarbon 38, 150.
944 Brown, E.T., Edmond, J.M., Raisbeck, G.M., Yiou, F., Kurz, M.D., Brook, E.J., 1991.
945 Examination of surface exposure ages of Antarctic moraines using in situ produced
946 ^{10}Be and ^{26}Al. Geochim. Cosmochim. Acta 55, 2269–2283.
947 https://doi.org/10.1016/0016-7037(91)90103-C
948 Chmeleff, J., von Blanckenburg, F., Kossert, K., Jakob, D., 2010. Determination of the
949 ^{10}Be half-life by multicollector ICP-MS and liquid scintillation counting. Nucl.
950 Instruments Methods Phys. Res. Sect. B Beam Interact. with Mater. Atoms 268,
951 192–199. https://doi.org/10.1016/J.NIMB.2009.09.012
952 Cockburn, H.A.P., Seidl, M.A., Summerfield, M.A., 1999. Quantifying denudation rates
953 on inselbergs in the central Namib Desert using in situ-produced cosmogenic ^{10}Be
954 and ^{26}Al. Geology 27, 399–402.
955 Codilean, A.T., Fenton, C.R., Fabel, D., Bishop, P., Xu, S., 2014. Discordance between
956 cosmogenic nuclide concentrations in amalgamated sands and individual fluvial
957 pebbles in an arid zone catchment. Quat. Geochronol. 19, 173–180.
958 https://doi.org/10.1016/j.quageo.2012.04.007
959 Corbett, L.B., Bierman, P.R., Rood, D.H., Caffee, M.W., Lifton, N.A., Woodruff, T.E.,
960 2017. Cosmogenic ^{26}Al /^{10}Be surface production ratio in Greenland. Geophys. Res.
961 Lett. 44, 1350–1359. https://doi.org/10.1002/2016GL071276
962 Dewald, A., Heinze, S., Jolie, J., Zilges, A., Dunai, T., Rethemeyer, J., Melles, M.,
963 Staubwasser, M., Kuczewski, B., Richter, J., Radtke, U., von Blanckenburg, F.,
964 Klein, M., 2013. CologneAMS, a dedicated center for accelerator mass spectrometry
965 in Germany. Nucl. Instruments Methods Phys. Res. Sect. B Beam Interact. with
966 Mater. Atoms 294, 18–23. https://doi.org/10.1016/J.NIMB.2012.04.030
967 Di Nicola, L., Strasky, S., Schlüchter, C., Salvatore, M.C., Akçar, N., Kubik, P.W.,
968 Christl, M., Kasper, H.U., Wieler, R., Baroni, C., 2009. Multiple cosmogenic
969 nuclides document complex Pleistocene exposure history of glacial drifts in Terra
970 Nova Bay (northern Victoria Land, Antarctica). Quat. Res. 71, 83–92.
971 Dunai, T.J., 2000. Scaling factors for production rates of in situ produced cosmogenic
972 nuclides: a critical reevaluation. Earth Planet. Sci. Lett. 176, 157–169.

973 Fenton, C.R., Niedermann, S., 2014. Surface exposure dating of young basalts (1–200 ka)
974 in the San Francisco volcanic field (Arizona, USA) using cosmogenic ^{3}He and ^{21}Ne.
975 Quat. Geochronol. 19, 87–105. https://doi.org/10.1016/J.QUAGEO.2012.10.003
976 Fenton, C.R., Mark, D.F., Barfod, D.N., Niedermann, S., Goethals, M.M., Stuart, F.M.,
977 2013. ^{40}Ar/^{39}Ar dating of the SP and Bar Ten lava flows AZ, USA: Laying the
978 foundation for the SPICE cosmogenic nuclide production-rate calibration project.
979 Quat. Geochronol. 18, 158–172. https://doi.org/10.1016/J.QUAGEO.2013.01.007
980 Fenton, C.R., Niedermann, S., Dunai, T., Binnie, S.A., 2019. The SPICE project:
981 Production rates of cosmogenic ^{21}Ne, ^{10}Be, and ^{14}C in quartz from the 72 ka SP
982 basalt flow, Arizona, USAu. Quat. Geochronol. 54, 101019.
983 https://doi.org/10.1016/J.QUAGEO.2019.101019
984 Fülöp, R.-H., Bishop, P., Fabel, D., Cook, G.T., Everest, J., Schnabel, C., Codilean, A.T.,
985 Xu, S., 2015. Quantifying soil loss with in-situ cosmogenic ^{10}Be and ^{14}C depth-
986 profiles. Quat. Geochronol. 27, 78–93.
987 https://doi.org/10.1016/J.QUAGEO.2015.01.003
988 Gärtner, A., Merchel, S., Niedermann, S., Braucher, R., ASTER-Team, Steier, P., Rugel,
989 G., Scharf, A., Le Bras, L., Linnemann, U., 2020. Nature does the averaging—in-situ
990 produced ^{10}Be, ^{21}Ne, and ^{26}Al in a very young river terrace. Geosciences 19, 237.
991 https://doi.org/10.3390/geosciences10060237
992 Glasser, N.F., Hughes, P.D., Fenton, C., Schnabel, C., Rother, H., 2012. ^{10}Be and ^{26}Al
993 exposure-age dating of bedrock surfaces on the Aran ridge, Wales: Evidence for a
994 thick Welsh Ice Cap at the Last Glacial Maximum. J. Quat. Sci. 27, 97-104.
995 https://doi.org/10.1002/jqs.1519
996 Goethals, M.M., Hetzel, R., Niedermann, S., Wittmann, H., Fenton, C.R., Kubik, P.W.,
997 Christl. M., von Blanckenburg, F., 2009. An improved experimental determination
998 of cosmogenic ^{10}Be/^{21}Ne and ^{26}Al/^{21}Ne production ratios in quartz. Earth Planet. Sci.
999 Lett. 284, 187-198.
1000 Gosse, J.C., Phillips, F.M., 2001. Terrestrial in situ cosmogenic nuclides: Theory and
1001 application. Quat. Sci. Rev. 20, 1475–1560. https://doi.org/10.1016/S0277-
1002 3791(00)00171-2
1003 Granger, D.E., 2006. A review of burial dating methods using ^{26}Al and ^{10}Be. In Siame,
1004 L.L., Bourlès, D.L., and Brown, E.T., eds., Application of cosmogenic nuclides to
1005 the stude of Earth surface processes: The practice and the potential: Geol. Soc. Of
1006 America Spec. Pap 415, 1-16.
1007 Granger, D.E., Fabel, D., Palmer, A.N., 2001. Pliocene- Pleistocene incision of the Green
1008 River, Kentucky, determined from radioactive decay of cosmogenic ^{26}Al and ^{10}Be in
1009 Mammoth Cave sediments. Geol. Soc. Am. Bull. 113, 825–836.
1010 Heisinger, B., Lal, D., Jull, A.J.T., Kubik, P., Ivy-Ochs, S., Knie, K., Nolte, E., 2002a.
1011 Production of selected cosmogenic radionuclides by muons: 2. Capture of negative
1012 muons. Earth Planet. Sci. Lett. 200, 357–369. https://doi.org/10.1016/S0012-
1013 821X(02)00641-6
1014 Heisinger, B, Lal, D., Jull, A.J.T., Kubik, P., Ivy-Ochs, S., Neumaier, S., Knie, K.,
1015 Lazarev, V., Nolte, E., 2002b. Production of selected cosmogenic radionuclides by
1016 muons: 1. Fast muons. Earth Planet. Sci. Lett. 200, 345–355.
1017 Hetzel, R., Niedermann, S., Ivy-Ochs, S., Kubik, P.W., Tao, M., Gao, B., 2002. ^{21}Ne
1018 versus ^{10}Be and ^{26}Al exposure ages of fluvial terraces: the influence of crustal Ne in

quartz. Earth Planet. Sci. Lett. 201, 575–591. https://doi.org/https://doi.org/10.1016/S0012-821X(02)00748-3

Hippe, K., Kober, F., Zeilinger, G., Ivy-Ochs, S., Kubik, P., Maden, C., Wieler, R., 2010. Do cosmogenic nuclides (^{10}Be, ^{14}C, ^{21}Ne, ^{26}Al) track late Quaternary climate changes on the Altiplano?, in: AGU Fall Meeting Abstracts.

Hippe, K., Kober, F., Zeilinger, G., Ivy-Ochs, S., Maden, C., Wacker, L., Kubik, P.W., Wieler, R., 2012. Quantifying denudation rates and sediment storage on the eastern Altiplano, Bolivia, using cosmogenic ^{10}Be, ^{26}Al, and in situ ^{14}C. Geomorphology 179, 58–70. https://doi.org/10.1016/J.GEOMORPH.2012.07.031

Hippe, K., Gordijn, T., Picotti, V., Hajdas, I., Jansen, J.D., Christl, M., Vockenhuber, C., Maden, C., Akçar, N., Ivy-Ochs, S., 2019. Fluvial dynamics and ^{14}C -^{10}Be disequilibrium on the Bolivian Altiplano. Earth Surf. Process. Landforms 44, 766–780.

Ivy-Ochs, S., Kerschner, H., Reuther, A., Maisch, M., Sailer, R., Schaefer, J., Kubik, P.W., Synal, H., Schlüchter, C., 2006. The timing of glacier advances in the northern European Alps based on surface exposure dating with cosmogenic ^{10}Be, ^{26}Al, ^{36}Cl, and ^{21}Ne. Spec. Pap. Soc. Am. 415, 43.

Ivy-Ochs, S., Kober, F., Alfimov, V., Kubik, P.W., Synal, H.-A., 2007. Cosmogenic ^{10}Be, ^{21}Ne and ^{36}Cl in sanidine and quartz from Chilean ignimbrites. Nucl. Instruments Methods Phys. Res. Sect. B Beam Interact. with Mater. Atoms 259, 588–594. https://doi.org/https://doi.org/10.1016/j.nimb.2007.03.001

Kelly, M.A., Lowell, T.V., Applegate, P.J., Phillips, F.M., Schaefer, J.M., Smith, C.A., Kim, H., Leonard, K.C., Hudson, A.M., 2015. A locally calibrated, late glacial ^{10}Be production rate from a low-latitude, high-altitude site in the Peruvian Andes. Quat. Geochronol. 26, 70–85. https://doi.org/10.1016/J.QUAGEO.2013.10.007

Klein, J., Giegengack, R., Middleton, R., Sharma, P., Underwood, J.R., Weeks, R.A., 1986. Revealing histories of exposure using in situ produced ^{26}Al and ^{10}Be in Libyan Desert glass. Radiocarbon 28, 547–555. https://doi.org/10.1017/s0033822200007700

Kober, F., Ivy-Ochs, S., Schlunegger, F., Baur, H., Kubik, P.W., Wieler, R., 2007. Denudation rates and a topography-driven rainfall threshold in northern Chile: Multiple cosmogenic nuclide data and sediment yield budgets. Geomorphology 83, 97–120. https://doi.org/https://doi.org/10.1016/j.geomorph.2006.06.029

Kober, F., Ivy-Ochs, S., Zeilinger, G., Schlunegger, F., Kubik, P.W., Baur, H., Wieler, R., 2009. Complex multiple cosmogenic nuclide concentration and histories in the arid Rio Lluta catchment, northern Chile. Earth Surf. Process. Landforms 34, 398–412.

Kober, F., Alfimov, V., Ivy-Ochs, S., Kubik, P.W., Wieler, R., 2011. The cosmogenic ^{21}Ne production rate in quartz evaluated on a large set of existing ^{21}Ne–^{10}Be data. Earth Planet. Sci. Lett. 302, 163–171. https://doi.org/https://doi.org/10.1016/j.epsl.2010.12.008

Kohl, C.., Nishiizumi, K., 1992. Chemical isolation of quartz for measurement of in-situ-produced cosmogenic nuclides. Geochim. Cosmochim. Acta 56, 3583–3587. https://doi.org/10.1016/0016-7037(92)90401-4

Korschinek, G., Bergmaier, A., Faestermann, T., Gerstmann, U.C., Knie, K., Rugel, G., Wallner, A., Dillmann, I., Dollinger, G., von Gostomski, C.L., Kossert, K., Maiti,

M., Poutivtsev, M., Remmert, A., 2010. A new value for the half-life of ^{10}Be by Heavy-Ion Elastic Recoil Detection and liquid scintillation counting. Nucl. Instruments Methods Phys. Res. Sect. B Beam Interact. with Mater. Atoms 268, 187–191. https://doi.org/10.1016/J.NIMB.2009.09.020

Kounov, A., Niedermann, S., De Wit, M.J., Codilean, A.T., Viola, G., Andreoli, M., Christl, M., 2015. Cosmogenic ^{21}Ne and ^{10}Be reveal a more than 2 Ma alluvial fan flanking the Cape Mountains, South Africa. South African J. Geol. 118, 129–144.

Kubik, P.W., Ivy-Ochs, S., Masarik, J., Frank, M., Schlüchter, C., 1998. ^{10}Be and ^{26}Al production rates deduced from an instantaneous event within the dendro-calibration curve, the landslide of Köfels, Ötz Valley, Austria. Earth Planet. Sci. Lett. 161, 231–241. https://doi.org/10.1016/S0012-821X(98)00153-8

Lal, D., 1991. Cosmic ray labeling of erosion surfaces: in situ nuclide production rates and erosion models. Earth Planet. Sci. Lett. 104, 424–439. https://doi.org/10.1016/0012-821X(91)90220-C

Lal, D., Jull, A.J.T., 2001. In-situ cosmogenic ^{14}C: Production and examples of its unique applications in studies of terrestrial and extraterrestrial processes. Radiocarbon 43, 731–742.

Larsen, P.L., 1996. In-situ production rates of cosmogenic ^{10}Be and ^{26}Al over the past 21,500 years determined from the terminal moraine of the Laurentide Ice Sheet, North-Central New Jersey. MS Thesis. University of Vermont.

Lifton, N., Sato, T., Dunai, T.J., 2014. Scaling in situ cosmogenic nuclide production rates using analytical approximations to atmospheric cosmic-ray fluxes. Earth Planet. Sci. Lett. 386, 149–160. https://doi.org/10.1016/J.EPSL.2013.10.052

Lifton, N., Caffee, M., Finkel, R., Marrero, S., Nishiizumi, K., Phillips, F.M., Goehring, B., Gosse, J., Stone, J., Schaefer, J., Theriault, B., Jull, A.J.T., Fifield, K., 2015. In situ cosmogenic nuclide production rate calibration for the CRONUS-Earth project from Lake Bonneville, Utah, shoreline features. Quat. Geochronol. 26, 56–69. https://doi.org/10.1016/J.QUAGEO.2014.11.002

Luna, L. V., Bookhagen, B., Niedermann, S., Rugel, G., Scharf, A., Merchel, S., 2018. Glacial chronology and production rate cross-calibration of five cosmogenic nuclide and mineral systems from the southern Central Andean Plateau. Earth Planet. Sci. Lett. 500, 242–253. https://doi.org/10.1016/J.EPSL.2018.07.034

Marrero, S.M., Phillips, F.M., Borchers, B., Lifton, N., Aumer, R., Balco, G., 2016. Cosmogenic nuclide systematics and the CRONUScalc program. Quat. Geochronol. 31, 160–187. https://doi.org/10.1016/J.QUAGEO.2015.09.005

Martin, L.C.P., Blard, P.-H., Lavé, J., Braucher, R., Lupker, M., Condom, T., Charreau, J., Mariotti, V., ASTER Team, Davy, E., 2015. In situ cosmogenic ^{10}Be production rate in the High Tropical Andes. Quat. Geochronol. 30, 54–68. https://doi.org/https://doi.org/10.1016/j.quageo.2015.06.012

McFadden, L. D., McDonald, E. V., Wells, S. G., Anderson, K., Quade, J., Forman, S. L., 1998. The vesicular layer and carbonate collars of desert soils and pavements: formation, age and relation to climate change. Geomorphology 24, 101-145. doi: 10.1016/S0169-555X(97)00095-0

McPhillips, D., Hoke, G.D., Liu-Zeng, J., Bierman, P.R., Rood, D.H., Niedermann, S., 2016. Dating the incision of the Yangtze River gorge at the First Bend using three-nuclide burial ages. Geophys. Res. Lett. 43, 101–110.

Miller, G.H., Briner, J.P., Lifton, N.A., Finkel, R.C., 2006. Limited ice-sheet erosion and complex exposure histories derived from in situ cosmogenic ^{10}Be, ^{26}Al, and ^{14}C on Baffin Island, Arctic Canada. Quat. Geochronol. 1, 74–85. https://doi.org/10.1016/J.QUAGEO.2006.06.011

Niedermann, S., Graf, T., Kim, J.S., Kohl, C.P., Marti, K., Nishiizumi, K., 1994. Cosmic-ray-produced ^{21}Ne in terrestrial quartz: the neon inventory of Sierra Nevada quartz separates. Earth Planet. Sci. Lett. 125, 341–355.

Nishiizumi, K., 2004. Preparation of ^{26}Al AMS standards. Nucl. Instruments Methods Phys. Res. Sect. B Beam Interact. with Mater. Atoms 223–224, 388–392. https://doi.org/10.1016/J.NIMB.2004.04.075

Nishiizumi, K., Winterer, E.L., Kohl, C.P., Klein, J., Middleton, R., Lal, D., Arnold, J.R., 1989. Cosmic ray production rates of ^{10}Be and ^{26}Al in quartz from glacially polished rocks. J. Geophys. Res. 94, 17907-17915. https://doi.org/10.1029/JB094iB12p17907

Nishiizumi, K., Kohl, C.P., Arnold, J.R., Klein, J., Fink, D., Middleton, R., 1991. Cosmic ray produced ^{10}Be and ^{26}Al in Antarctic rocks: exposure and erosion history. Earth Planet. Sci. Lett. 104, 440–454. https://doi.org/10.1016/0012-821X(91)90221-3

Nishiizumi, K., Caffee, M.W., Finkel, R.C., Brimhall, G., Mote, T., 2005. Remnants of a fossil alluvial fan landscape of Miocene age in the Atacama Desert of northern Chile using cosmogenic nuclide exposure age dating. Earth Planet. Sci. Lett. 237, 499–507. https://doi.org/10.1016/J.EPSL.2005.05.032

Nishiizumi, K., Imamura, M., Caffee, M.W., Southon, J.R., Finkel, R.C., McAninch, J., 2007. Absolute calibration of ^{10}Be AMS standards. Nucl. Instruments Methods Phys. Res. Sect. B Beam Interact. with Mater. Atoms 258, 403–413.

Phillips, F.M., Kelly, M.A., Hudson, A.M., Stone, J.O.H., Schaefer, J., Marrero, S.M., Fifield, L.K., Finkel, R., Lowell, T., 2016. CRONUS-Earth calibration samples from the Huancané II moraines, Quelccaya ice cap, Peru. Quat. Geochronol. 31, 220–236.

Reedy, R.C., Tuniz, C., Fink, D., 1994. Report on the workshop on production rates of terrestrial in-situ-produced cosmogenic nuclides. Nucl. Instruments Methods Phys. Res. Sect. B Beam Interact. with Mater. Atoms 92, 335–339.

Repka, J.L., Anderson, R.S., Finkel, R.C., 1997. Cosmogenic dating of fluvial terraces, Fremont River, Utah. Earth Planet. Sci. Lett. 152, 59–73. https://doi.org/10.1016/S0012-821X(97)00149-0

Rittenour, T.M., Riggs, N.R., Kennedy, L.E., 2012. Application of single-grain OSL to date quartz xenocrysts within a basalt flow, San Francisco volcanic field, northern Arizona, USA. Quat. Geochronol. 10, 300–307.

Rolfe, C.J., Hughes, P.D., Fenton, C.R., Schnabel, C., Xu, S., Brown, A.G., 2012. Paired ^{26}Al and ^{10}Be exposure ages from Lundy: new evidence for the extent and timing of Devensian glaciation in the southern British Isles. Quat. Sci. Rev. 34, 61-73. https://doi.org/10.1016/j.quascirev.2012.04.003

Schaller, M., von Blanckenburg, F., Hovius, N., Kubik, P.W., 2001. Large-scale erosion rates from in situ-produced cosmogenic nuclides in European river sediments. Earth Planet. Sci. Lett. 188, 441–458. https://doi.org/10.1016/S0012-821X(01)00320-X

Schildgen, T., Dethier, D.P., Bierman, P., Caffee, M., 2002. ^{26}Al and ^{10}Be dating of late Pleistocene and Holocene fill terraces: a record of fluvial deposition and incision, Colorado Front Range. Earth Surf. Process. Landforms 27, 773–787.

Skov, D.S., Egholm, D.L., Jansen, J.D., Sandiford, M., Knudsen, M.F., 2019. Detecting

landscape transience with in situ cosmogenic ^{14}C and ^{10}Be. Quat. Geochronol. 54, 101008. https://doi.org/10.1016/J.QUAGEO.2019.101008

Stone, J.O., 2000. Air pressure and cosmogenic isotope production. J. Geophys. Res. Solid Earth 105, 23753–23759. https://doi.org/10.1029/2000jb900181

Stone, J., Fifield, K., Beer, J., Vonmoos, M., Obrist, C., Grajcar, M., Kubik, P., Muscheler, R., Finkel, R., Caffee, M., 2004. Co-precipitated silver–metal oxide aggregates for accelerator mass spectrometry of ^{10}Be and ^{26}Al. Nucl. Instruments Methods Phys. Res. Sect. B Beam Interact. with Mater. Atoms 223–224, 272–277. https://doi.org/10.1016/J.NIMB.2004.04.055

Summerfield, M.A., Stuart, F.M., Cockburn, H.A.P., Sugden, D.E., Denton, G.H., Dunai, T., Marchant, D.R., 1999. Long-term rates of denudation in the Dry Valleys, Transantarctic Mountains, southern Victoria Land, Antarctica based on in-situ-produced cosmogenic ^{21}Ne. Geomorphology 27, 113–129. https://doi.org/https://doi.org/10.1016/S0169-555X(98)00093-2

Tschudi, S., Schäfer, J.M., Zhao, Z., Wu, X., Ivy-Ochs, S., Kubik, P.W., Schlüchter, C., 2003. Glacial advances in Tibet during the Younger Dryas? Evidence from cosmogenic ^{10}Be, ^{26}Al, and ^{21}Ne. J. Asian Earth Sci. 22, 301–306. https://doi.org/10.1016/S1367-9120(03)00035-X

Vermeesch, P., 2007. CosmoCalc: An Excel add-in for cosmogenic nuclide calculations. Geochem. Geophys. Geosyst. 8, Q08003. https://doi.org/10.1029/2006GC001530

Vermeesch, P., Fenton, C.R., Kober, F., Wiggs, G.F.S., Bristow, C.S., Xu, S., 2010. Sand residence times of one million years in the Namib Sand Sea from cosmogenic nuclides. Nat. Geosci. 3, 862–865. https://doi.org/10.1038/ngeo985

Wilson, S.R., Ward, G.K.,1978. Procedures for comparing and combining radiocarbon age determinations: a critique. Archaeometry 20, 19–31. https://doi.org/10.1111/j.1475-4754.1978.tb00208.x

White, D., Fülöp, R.-H., Bishop, P., Mackintosh, A., Cook, G., 2011. Can in-situ cosmogenic ^{14}C be used to assess the influence of clast recycling on exposure dating of ice retreat in Antarctica? Quat. Geochronol. 6, 289–294. https://doi.org/10.1016/J.QUAGEO.2011.03.004

Young, N.E., Lamp, J., Koffman, T., Briner, J.P., Schaefer, J., Gjermundsen, E.F., Linge, H., Zimmerman, S., Guilderson, T.P., Fabel, D., Hormes, A., 2018. Deglaciation of coastal south-western Spitsbergen dated with in situ cosmogenic ^{10}Be and ^{14}C measurements. J. Quat. Sci. 33, 763–776.

Zehfuss, P.H., Bierman, P.R., Gillespie, A.R., Burke, R.M., Caffee, M.W., 2001. Slip rates on the Fish Springs fault, Owens Valley, California, deduced from cosmogenic ^{10}Be and ^{26}Al and soil development on fan surfaces. Geol. Soc. Am. Bull. 113, 241–255.

Supplementary Data

Table SD1. Cosmogenic $^{26}Al/^{10}Be$ ratios in quartz normalized to KNSTD/07KNSTD as calculated and reported in Corbett et al. (2017).

Reference	$^{26}Al/^{10}Be$
Klein et al. (1986)	7.7
Nishiizumi et al. (1989)	6.6 ± 0.5
Lal (1991)	6.7 ± 0.4
Nishiizumi et al. (1991)	6.9
Brown et al. (1991)	6.2 ± 1.0
Reedy et al. (1994)	7.9 ± 0.8
Larsen (1996)	6.4 ± 0.2
Kubik et al. (1998)	6.53 ± 0.43
Nishiizumi et al. (2005)	6.7
Goethals et al. (2009b)	7.76 ± 0.49
Corbett et al. (2017)	7.3 ± 0.3
Luna et al. (2018)	5.87 ± 0.24
Phillips et al. (2016) (PERU)	6.74 ± 0.34
Borchers et al. (2016) (SCOT)	7.19 ± 0.18 [a]
Lifton et al. (2015) (PPT)	6.53 ± 0.14 [a]

Note: The $^{26}Al/^{10}Be$ values include spallogenic and muogenic ^{26}Al and ^{10}Be, and thus relate to the total reference production-rate ratios. Values are normalized to KNSTD/07KNSTD of Nishiizumi (2004) and Nishiizumi et al. (2007).

[a] Calculated in this study using data from the primary calibration data sets for ^{26}Al and ^{10}Be production rates in Borchers et al. (2016) and the ICE-D Production Rate Calibration Data database (http://calibration.ice-d.org/).

Table SD2. Local production-rate ratios calculated in this study for cross-calibrated cosmogenic ^{10}Be, ^{26}Al, and ^{14}C concentrations in Promontory Point (PPT) quartz samples.

	$^{26}Al/^{10}Be$[a]	$^{26}Al/^{14}C$
Arithmetical mean ± $2\sigma_{SD}$	6.53 ± 1.31	1.90 ± 0.33
Error weighted mean ± $2\sigma_{\bar{x}}$	6.53 ± 0.14	1.93 ± 0.05

Note: Original data are reported in Lifton et al. (2015) and are a product of a CRONUS-Earth cosmogenic nuclide production rate calibration project. Standard deviation and standard error are represented as $2\sigma_{SD}$ and $2\sigma_{\bar{x}}$, respectively.

[a] The $^{26}Al/^{10}Be$ values are based on the total reference local production-rate ratios integrated over 18.36 ka. Values are normalized to KNSTD/07KNSTD of Nishiizumi (2004) and Nishiizumi et al. (2007)

Table SD3. Spallation production-rate ratios calculated from spallation production rates for cosmogenic ^{10}Be, ^{14}C, ^{21}Ne, and ^{26}Al in quartz as reported in CRONUS-Earth studies by Borchers et al (2016) and Marrero et al (2016).

Scaling method used in Borchers et al. (2016) and Marrero et al. (2016)	$^{26}Al_{sp}/^{10}Be_{sp}$	$^{26}Al_{sp}/^{14}C_{sp}$	$^{26}Al_{sp}/^{21}Ne$
St	6.97	2.28	1.68
Lm	6.98	2.29	--
Sf	7.00	2.25	1.69
Sa	7.28	2.24	--

Note: -- indicates no data available for these scaling methods in Borchers et al. (2016) or Marrero et al. (2016). No uncertainties are reported for the production ratios, because Borchers et al. (2016) state they "cannot infer statistically justifiable production rate uncertainties from the fitting exercise."

Table SD4. Measured cosmogenic ^{26}Al concentrations in SPICE quartz samples and associated laboratory blanks. All AMS measurements were made at the University of Cologne.

Sample ID	Quartz mass (g)	^{27}Al atoms (10^{19}) measured in the dissolved, spiked sample	^{26}Al /^{27}Al (10^{-13}) [a]	2σ uncertainty (10^{-13}) [a]	Blank corrected ^{26}Al concentration (10^6 at/g)[b]	2σ uncertainty (10^6 at/g)[b]	2σ uncertainty (%)	Error-weighted mean ^{26}Al concentration (10^6 at/g)[c]	2σ uncertainty (10^6 at/g)[c]
SPICE-A1	2.1608	3.86	3.37	0.45	5.9	0.9	15		
SPICE-A2	2.0707	3.81	3.18	0.42	5.8	0.9	15		
SPICE-A3	2.0711	3.89	3.14	0.42	5.8	0.9	15	5.7	0.9
SPICE-A3 [c]	2.0559	3.79	3.13	0.43	5.7	0.9	16		
SPICE-A4	2.1188	3.80	3.14	0.45	5.6	0.9	16	5.8	0.9
SPICE-A4 [c]	2.0803	3.92	3.28	0.48	6.1	1.0	16		
SPICE-A5	2.1358	3.88	3.01	0.70	5.4	1.3	24		
SPICE-A6	2.1112	3.85	3.58	0.57	6.5	1.1	17	6.1	1.1
SPICE-A6 [c]	2.0919	3.91	3.11	0.53	5.8	1.1	19		
SPICE-A7	2.0676	3.87	3.15	0.58	5.9	1.2	20		
SPICE-A8	2.1340	3.85	3.49	0.55	6.3	1.1	17	5.8	1.1
SPICE-A8 [c]	2.1391	3.86	3.00	0.54	5.4	1.0	19		
SPICE-A9	2.0503	3.84	2.92	0.47	5.4	1.0	18		
SPICE-A10	2.0525	3.95	2.95	0.55	5.7	1.1	20		
Process blanks									
Blank[d]		3.35	0.042	0.049					
Blank[d]		3.31	0.070	0.053					
Blank[e]		3.31	0.055	0.055					
Blank[e]		3.30	0.033	0.065					

Note: ^{26}Al concentrations in this table are not scaled to sea level and high latitude (SLHL). All uncertainties are **2σ**.

[a] ^{26}Al /^{27}Al ratios are normalized using the standards of Nishiizumi (2004). Standards and their nominal values used in these AMS measurements are KN01-5-3 (^{26}Al /^{27}Al = 4.99×10^{-13}) and KN01-4-3 (^{26}Al /^{27}Al = 1.065×10^{-11}). Uncertainties in the ^{26}Al /^{27}Al measurements include the uncertainty in the number of ^{26}Al counts and any scatter in the standards. The AMS standardization parameter KNSTD in the online calculator of Balco et al. (2008) indicates internal ^{26}Al /^{27}Al normalization to the Nishiizumi (2004) standard and is used with ^{26}Al /^{27}Al data from CologneAMS in the online calculator.

[b] Blank subtractions are between 0.4% and 1.6 % of the total ^{26}Al measured. Uncertainties of the blank corrected ^{26}Al concentrations include the propagated uncertainties in the total number of ^{26}Al atoms in the sample and the uncertainty of the ^{26}Al atoms in the blank, estimated from the mean and standard deviation of the pair of blank measurements

1238 included in each sample batch. The uncertainty of the number of ^{26}Al atoms in the sample includes an estimated 3.5 % (1 s.d.) uncertainty in the mass of ^{27}Al in the sample,
1239 propagated with the uncertainty of the AMS ^{26}Al /^{27}Al measurement.
1240 [c] Error-weighted means and estimated standard deviations of the means of duplicate AMS measurements are calculated for samples –A3, -A4, -A6, and –A8, after Wilson and
1241 Ward (1978).
1242 [d] Processed alongside samples SPICE-A1 through SPICE-A5.
1243 [e] Processed alongside samples SPICE-A6 through SPICE-A10.
1244

1245

Table SD5. Error weighted means and standard error ($2\sigma_{\bar{x}}$) of local production-rate ratios and production-rate ratios of spallogenic $^{26}Al_{sp}$ to total reference ^{21}Ne and spallogenic $^{10}Be_{sp}$ and $^{14}C_{sp}$ in SP-flow quartz.

Sample ID	$^{26}Al/^{21}Ne$[a]	2σ uncertainty[a]	$^{26}Al/^{10}Be$[a]	2σ uncertainty[a]	$^{26}Al/^{14}C$[a]	2σ uncertainty[a]	**(a) Scaled with St scaling factors** $^{26}Al_{sp}/^{21}Ne$	2σ uncertainty	$^{26}Al_{sp}/^{10}Be_{sp}$	2σ uncertainty	$^{26}Al_{sp}/^{14}C_{sp}$	2σ uncertainty
SPICE-A1	1.56	0.29	6.7	1.2	2.175	0.40	1.51	0.35	6.7	1.5	2.54	0.61
SPICE-A2	1.41	0.26	6.3	1.2	2.290	0.44	1.36	0.31	6.3	1.5	2.71	0.66
SPICE-A3	1.53	0.28	6.7	1.2	2.111	0.40	1.48	0.34	6.7	1.6	2.44	0.60
SPICE-A4	1.56	0.28	6.8	1.3	2.312	0.46	1.52	0.36	6.8	1.7	2.72	0.70
SPICE-A5	1.49	0.29	6.6	1.2	2.288	0.46	1.44	0.35	6.6	1.6	2.70	0.69
SPICE-A6	1.74	0.37	7.4	1.5	2.255	0.48	1.69	0.46	7.4	2.0	2.61	0.74
SPICE-A7	1.50	0.41	6.5	1.7	1.608	0.42	1.45	0.53	6.5	2.4		
SPICE-A8	1.44	0.29	6.8	1.4	2.740	0.62	1.40	0.38	6.7	1.9	3.34	1.00
SPICE-A9	1.55	0.38	6.8	1.4	3.359	0.81	1.50	0.43	6.8	1.9		
SPICE-A10	1.41	0.31	6.6	1.5	2.432	0.57	1.37	0.40	6.5	2.0	2.88	0.91
Average[b]	**1.51**	**0.13** ($2\sigma_{\bar{x}}$)	**6.7**	**0.6** ($2\sigma_{\bar{x}}$)	**2.23**	**0.20** ($2\sigma_{\bar{x}}$)	**1.46**	**0.14** ($2\sigma_{\bar{x}}$)	**6.7**	**0.7** ($2\sigma_{\bar{x}}$)	**2.67**	**0.29** ($2\sigma_{\bar{x}}$)

[a] Ratios are based on local, unscaled production rates. No scaling factors were used in these calculations.

[b] This is an error-weighted mean of all ten samples, except for values using ^{14}C, for which SPICE-A7 and –A9 ^{14}C values are excluded as outliers (Fenton et al., 2019). The 2σ uncertainty is the standard error on the mean and includes the uncertainty on the $^{40}Ar/^{39}Ar$ age or radiocarbon half-life.

(b) Scaled with *Sf* scaling factors						
Sample ID	$^{26}Al_{sp}/^{21}Ne$	2σ uncertainty[a]	$^{26}Al_{sp}/^{10}Be_{sp}$	2σ uncertainty[a]	$^{26}Al_{sp}/^{14}C_{sp}$	2σ uncertainty
SPICE-A1	1.55	0.38	6.7	1.7	2.27	0.64
SPICE-A2	1.40	0.34	6.3	1.7	2.41	0.70
SPICE-A3	1.52	0.37	6.7	1.8	2.19	0.63
SPICE-A4	1.55	0.38	6.8	1.9	2.43	0.74
SPICE-A5	1.48	0.38	6.6	1.8	2.41	0.74
SPICE-A6	1.73	0.50	7.4	2.2	2.34	0.75
SPICE-A7	1.49	0.56	6.5	2.5		
SPICE-A8	1.43	0.40	6.7	2.0	2.96	1.04
SPICE-A9	1.54	0.49	6.8	2.1		
SPICE-A10	1.40	0.42	6.5	2.1	2.57	0.91
Average [b]	**1.50**	**0.15 ($2\sigma_{\bar{x}}$)**	**6.7**	**0.7 ($2\sigma_{\bar{x}}$)**	**2.39**	**0.29 ($2\sigma_{\bar{x}}$)**
(c) Scaled with *Sa* scaling factors						
Sample ID	$^{26}Al_{sp}/^{10}Be_{sp}$	2σ uncertainty	$^{26}Al_{sp}/^{14}C_{sp}$	2σ uncertainty		
SPICE-A1	6.9	1.8	2.23	0.63		
SPICE-A2	6.5	1.7	2.37	0.69		
SPICE-A3	6.9	1.8	2.15	0.62		
SPICE-A4	7.0	1.9	2.38	0.72		
SPICE-A5	6.8	1.8	2.37	0.72		
SPICE-A6	7.6	2.3	2.30	0.73		
SPICE-A7	6.7	2.5				
SPICE-A8	6.9	2.1	2.91	1.02		
SPICE-A9	7.0	2.1				
SPICE-A10	6.7	2.2	2.52	0.89		
Average [b]	**6.9**	**0.7 ($2\sigma_{\bar{x}}$)**	**2.35**	**0.29 ($2\sigma_{\bar{x}}$)**		

Table SD6. *St*, *Sf*, and *Sa* scaling factors calculated for calibration sites on the SP lava flow.

	^{26}Al	^{26}Al	^{26}Al	^{26}Al	^{26}Al	^{26}Al
Sample ID	***St*** scaling factor for fast and slow muons [a]	***St*** scaling factor for neutron spallation [a]	***Sf*** scaling factor for fast and slow muons [b]	***Sf*** scaling factor for neutron spallation [b]	***Sa*** scaling factor for fast and slow muons [b]	***Sa*** scaling factor for neutron spallation [b]
SPICE-A1	1.99	3.52	1.51	3.86	1.51	3.91
SPICE-A2	1.97	3.45	1.50	3.78	1.50	3.83
SPICE-A3	1.97	3.45	1.50	3.79	1.50	3.84
SPICE-A4	1.96	3.44	1.50	3.77	1.50	3.82
SPICE-A5	1.96	3.43	1.49	3.76	1.49	3.81
SPICE-A6	1.94	3.38	1.49	3.70	1.49	3.75
SPICE-A7	1.96	3.43	1.49	3.76	1.49	3.81
SPICE-A8	1.94	3.38	1.49	3.70	1.49	3.75
SPICE-A9	1.97	3.45	1.50	3.79	1.50	3.84
SPICE-A10	1.96	3.43	1.49	3.76	1.49	3.81

[a] The scaling factors were determined using CRONUSCalc (Marrero et al., 2016). Scaling factors are time independent.

[b] The scaling factors were determined using the mmc1 Matlab code of Lifton et al. (2014). Scaling factors are time-dependent. *Sf* and *Sa* scaling factors are integrated over the past 72 ka.

Complementary Quartz Data from Appendix B (Supplementary Data) of Fenton et al. (2019): The SPICE Project: Production rates of cosmogenic ^{21}Ne, ^{10}Be, and ^{14}C in quartz from the 72 ka SP basalt flow, Arizona, USA)

Table B1. ^{4}He and ^{20}Ne concentrations (cm^3 STP/g), Ne isotope ratios and excess ^{21}Ne (^{21}Ne$_{ex}$) concentrations (10^6 at/g) for stepwise heating extractions of quartz samples from SP Flow, Arizona. Data from crushing extractions of samples SPICE-A4 and –A8 are shown as well. Error limits are 2σ.

Sample Weight	T °C	^{4}He 10^{-8} cm^3/g	^{20}Ne 10^{-12} cm^3/g	^{22}Ne/^{20}Ne 10^{-2}	^{21}Ne/^{20}Ne 10^{-2}	^{21}Ne$_{ex}$[a] 10^{6} at/g
SPICE-A1	400	-	44.1	10.67	0.516	2.60
0.48040 g			±2.5	±0.19	±0.025	±0.32
	800	-	40.6	10.30	0.412	1.27
			±2.5	±0.22	±0.022	±0.25
	1200	-	0.43	9.1	0.71	0.047
			$^{+0.56}_{-0.43}$	±4.9	±0.55	±0.022
	Total	-	85.1	10.49	0.467	3.87
			±3.6	±0.15	±0.017	±0.41
SPICE-A2	400	-	37.4	10.50	0.477	1.82
0.47372 g			±2.2	±0.23	±0.020	±0.22
	800	-	31.3	10.76	0.576	2.35
			±2.1	±0.24	±0.038	±0.34
	1200	-	0.31	11.0	0.59	0.024
			$^{+0.65}_{-0.31}$	±5.3	$^{+0.98}_{-0.59}$	$^{+0.063}_{-0.024}$
	Total	-	69.0	10.62	0.522	4.17
			±3.1	±0.17	±0.021	±0.40
SPICE-A3	400	0.0126	51.9	10.74	0.508	2.95
0.48278 g		±0.0014	±2.8	±0.10	±0.021	±0.32
	600	0.0286	4.67	10.87	0.92	0.786
		±0.0021	±0.72	±0.35	±0.11	±0.097
	800	0.0059	4.29	10.19	0.367	0.082
		±0.0013	±0.92	±0.53	±0.053	±0.059
	1200	0.0018	1.17	11.5	0.42	0.101
		$^{+0.0045}_{-0.0018}$	±0.66	±1.1	±0.24	±0.060

	Total	0.0489 $^{+0.0053}_{-0.0034}$	62.0 ±3.1	10.73 ±0.10	0.528 ±0.021	3.82 ±0.34
SPICE-A4	Crushed	0.01505 ±0.00092	5.84 ±0.34	10.41 ±0.34	0.315 ±0.022	-
1.00778 g						
0.80032 g	400	-	0.55 ±0.39	19.5 ±6.5	8.4 ±5.7	1.20 ±0.16
	800	-	11.93 ±0.87	11.30 ±0.18	1.098 ±0.059	2.57 ±0.21
	1200	-	7.28 ±0.60	10.63 ±0.37	0.328 ±0.032	0.063 ±0.063
	Total	-	19.8 ±1.1	11.28 ±0.30	1.02 ±0.22	3.77 ±0.26

Table B1 (cont.)

Sample Weight	T *°C*	^{4}He 10^{-8} *cm^3/g*	^{20}Ne 10^{-12} *cm^3/g*	^{22}Ne/^{20}Ne 10^{-2}	^{21}Ne/^{20}Ne 10^{-2}	^{21}Ne$_{ex}$ 10^{6} *at/g*
SPICE-A5	400	-	44.0	10.59	0.447	1.78
0.48470 g			±2.5	±0.21	±0.025	±0.31
	800	-	25.7	10.97	0.588	2.01
			±1.7	±0.28	±0.037	±0.27
	1200	-	0.14	7	1.0	0.026
			$^{+0.63}_{-0.14}$	$^{+19}_{-7}$	$^{+3.6}_{-1.0}$	$^{+0.043}_{-0.026}$
	Total	-	69.8	10.72	0.500	3.80
			±3.1	±0.18	±0.023	±0.41
SPICE-A6	400	0.0096	50.4	10.60	0.492	2.66
0.48494 g		±0.0017	±2.7	±0.13	±0.026	±0.37
	800	0.857	10.2	10.56	0.635	0.92
		±0.043	±1.1	±0.47	±0.058	±0.15
	1200	0.262	0.39	10.3	0.55	0.068
		±0.014	$^{+0.66}_{-0.39}$	±5.4	±0.49	±0.024
	Total	1.129	61.0	10.59	0.516	3.56
		±0.045	±3.0	±0.14	±0.024	±0.40
SPICE-A7	400	0.0062	64.2	10.54	0.466	2.94
0.47508 g		±0.0018	±3.4	±0.13	±0.025	±0.45
	800	0.674	6.54	10.45	0.699	0.71
		±0.034	±0.99	±0.76	±0.078	±0.11
	1200	0.0120	0.56	10.3	0.28	0.035
		±0.0022	$^{+0.66}_{-0.56}$	±3.6	$^{+0.45}_{-0.28}$	$^{+0.059}_{-0.035}$
	Total	0.692	71.3	10.53	0.486	3.65
		±0.034	±3.6	±0.14	±0.024	±0.46
SPICE-A8	Crushed	0.0753	23.6	10.04	0.297	-
1.00802 g		±0.0039	±1.8	±0.17	±0.025	
0.80998 g	400	-	1.10	11.5	1.93	0.483
			±0.40	±1.4	±0.61	±0.080
	800	-	57.7	10.29	0.530	3.62
			±3.1	±0.19	±0.017	±0.33

1200	-	19.3	9.93	0.321	0.13
		±1.1	±0.24	±0.038	$^{+0.20}_{-0.13}$
Total	-	78.1	10.22	0.498	4.11
		±3.3	±0.15	±0.020	±0.34
SPICE-A9	400	0.0148	55.8	10.68	0.498	3.03
0.46248 g		±0.0019	±3.0	±0.15	±0.036	±0.56
	800	1.167	11.8	10.34	0.539	0.77
		±0.059	±1.2	±0.35	±0.064	±0.20
	1200	0.0215	0.81	9.1	0.38	0.032
		±0.0029	±0.68	±2.5	±0.26	$^{+0.054}_{-0.032}$
	Total	1.203	68.4	10.60	0.504	3.80
		±0.059	±3.3	±0.14	±0.032	±0.60

Table B1 (cont.)

Sample Weight	T °C	^{4}He 10^{-8} cm^3/g	^{20}Ne 10^{-12} cm^3/g	$^{22}Ne/^{20}Ne$ 10^{-2}	$^{21}Ne/^{20}Ne$ 10^{-2}	$^{21}Ne_{ex}$ 10^{6} at/g
SPICE-A10	400	-	28.3	10.39	0.444	1.12
0.48178 g			±1.7	±0.23	±0.034	±0.26
	800	-	38.3	10.71	0.600	3.12
			±2.4	±0.20	±0.018	±0.24
	1200	-	0.85	8.5	0.36	0.013
			±0.65	±3.0	±0.27	$^{+0.062}_{-0.013}$
	Total	-	67.5	10.55	0.532	4.24
			±3.0	±0.16	±0.018	±0.36
10SPC01	400	0.0034	4.07	10.21	0.53	0.26
0.52770 g		±0.0016	±0.71	±0.42	±0.10	±0.10
	800	0.246	36.9	10.43	0.686	3.86
		±0.012	±2.5	±0.16	±0.036	±0.42
	1200	0.0384	19.0	10.00	0.299	0.01
		±0.0041	±1.4	±0.17	±0.045	$^{+0.23}_{-0.01}$
	Total	0.288	60.0	10.28	0.553	4.12
		±0.013	±3.0	±0.12	±0.028	±0.43
10SPC06	400	0.0019	1.29	11.9	2.8	0.86
0.50342 g		±0.0017	±0.65	±1.1	±1.3	±0.17
	800	0.195	22.6	10.37	0.754	2.79
		±0.010	±1.8	±0.33	±0.030	±0.22
	1200	0.186	7.82	9.87	0.323	0.056
		±0.010	±0.87	±0.58	±0.039	$^{+0.083}_{-0.056}$
	Total	0.383	31.7	10.31	0.731	3.65
		±0.014	±2.1	±0.28	±0.073	±0.28
10SPC07	400	0.225	73.8	10.48	0.4446	2.95
0.73352 g		±0.012	±4.3	±0.12	±0.0082	±0.23
	600	7.94	21.1	10.94	0.514	1.24
		±0.40	±1.3	±0.15	±0.023	±0.15
	800	7.03	39.3	10.35	0.309	0.13
		±0.35	±2.5	±0.11	±0.020	$^{0.21}_{-0.13}$

	1200	1.172	10.11	10.56	0.395	0.269
		±0.059	±0.80	±0.21	±0.036	±0.099
	Total	16.37	144.3	10.52	0.4143	4.32
		±0.53	±5.2	±0.07	±0.0084	$^{+0.35}_{-0.30}$

[a] $^{21}Ne_{ex}$ was calculated relative to the atmospheic $^{21}Ne/^{20}Ne$ ratio of 0.002959 (Eberhardt et al., 1965). $^{21}Ne_{ex}$ contributions from 1200°C steps are generally small and are not included in totals (Niedermann, 2002).

Table B2. Measured cosmogenic ^{10}Be concentrations in SPICE quartz samples and associated laboratory blanks. All AMS measurements were made at the University of Cologne.

Sample ID	Quartz mass (g)	^{9}Be added in spike (10^{19} atoms)	^{10}Be/^{9}Be (10^{-13}) [a]	2σ uncertainty (10^{-13}) [a]	Blank corrected ^{10}Be concentration (10^{5} at/g)[b]	2σ uncertainty (10^{5} at/g)[b]	2σ uncertainty (%)	Error-weighted mean ^{10}Be concentration (10^{5} at/g)[c]	2σ uncertainty (10^{5} at/g)[c]
SPICE-A1	2.1608	1.691	1.15	0.10	8.86	0.78	8.8		
SPICE-A2	2.0707	1.687	1.14	0.10	9.11	0.85	9.3		
SPICE-A3	2.0711	1.651	1.09	0.09	8.49	0.76	8.9	8.58 [c]	0.76
SPICE-A3 [c]	2.0559	1.691	1.07	0.09	8.67	0.76	8.8		
SPICE-A4	2.1188	1.689	1.07	0.09	8.37	0.76	9.1	8.48 [c]	0.77
SPICE-A4 [c]	2.0803	1.695	1.07	0.09	8.59	0.78	9.1		
SPICE-A5	2.1358	1.694	1.06	0.09	8.24	0.76	9.2		
SPICE-A6	2.1112	1.691	1.03	0.09	8.08	0.75	9.3	8.28 [c]	0.76
SPICE-A6 [c]	2.0919	1.695	1.07	0.09	8.49	0.77	9.1		
SPICE-A7	2.0676	1.700	1.11	0.10	8.94	0.80	9.0		
SPICE-A8	2.1340	1.693	1.11	0.10	8.63	0.79	9.1		
SPICE-A8 [c]	2.1391	1.689	1.11	0.10	8.56	0.79	9.3	8.60 [c]	0.79
SPICE-A9	2.0503	1.702	1.05	0.09	8.52	0.78	9.2		
SPICE-A10	2.0525	1.696	1.05	0.09	8.44	0.77	9.2		
Process blanks									
Blank[d]		1.696	0.0155	0.0081					
Blank[d]		1.704	0.0235	0.0097					
Blank[e]		1.695	0.0175	0.0094					
Blank[e]		1.697	0.0304	0.0137					

Note: ^{10}Be concentrations in this table are not scaled to sea level and high latitude (SLHL). All uncertainties are **2σ**. A spike of approximately 250 microgram of ^{9}Be were added to each sample. Natural amounts of ^{9}Be were not measured in SP flow quartz samples.

[a] ^{10}Be/^{9}Be values are normalized using the standards of Nishiizumi et al. (2007). Standards and their nominal values used in these AMS measurements are KN01-6-2 (^{10}Be/^{9}Be = 5.35×10^{-13}) and KN01-5-1 (^{10}Be/^{9}Be = 2.709×10^{-11}). Uncertainties in our ^{10}Be/^{9}Be measurements include uncertainty in the number of counts and any scatter in the standards. The AMS standardization parameter 07KNSTD in the online calculator of Balco et al. (2008) indicates internal ^{10}Be/^{9}Be normalization to the Nishiizumi et al. (2007) standard, and is used with ^{10}Be/^{9}Be data from CologneAMS in the online calculator.

[b] Blank subtractions are between 1.7% to 2.2 % of the total ^{10}Be measured. Uncertainties in the blank corrected ^{10}Be concentrations include the propagated uncertainties in the total number of ^{10}Be atoms in the sample and the uncertainty in the ^{10}Be atoms in the blank, estimated from the mean and standard deviation of the pair of blank measurements included

in each sample batch. The uncertainty in the number of ^{10}Be atoms in the sample includes an estimated 1% (1 s.d.) uncertainty in the mass of ^{9}Be added to the sample, propagated with the uncertainty in the AMS ^{10}Be/^{9}Be measurement.

[c] Error-weighted (pooled) means and standard deviation of the means of duplicate AMS measurements are calculated for samples –A3, -A4, -A6, and –A8 after Wilson and Ward (1978).

[d] Processed alongside samples SPICE-A1 through SPICE-A5.

[e] Processed alongside samples SPICE-A6 through SPICE-A10.

Table B3. Measured cosmogenic ^{14}C concentrations in SPICE quartz samples and associated laboratory blanks. All AMS measurements were made at the University of Cologne.

Sample ID	Mass sample (g)	µg C [a]	$^{14}C/^{12}C$ (10^{-13}) [b]	2σ uncertainty (10^{-13}) [b]	^{14}C (10^5 atoms) [c]	2σ uncertainty (10^5 atoms)	Blank-corrected ^{14}C concentration (10^5 at/g) [d]	2σ uncertainty (10^5 at/g) [d]
SPICE-A1	1.001	6.89	10.70	0.37	3.70	0.12	3.18	0.33
SPICE-A2	0.989	7.67	8.90	0.28	3.42	0.10	2.94	0.32
SPICE-A3	0.957	4.67	11.30	0.53	3.55	0.12	3.18	0.33
SPICE-A4	0.984	6.82	10.40	0.33	3.39	0.12	2.93	0.33
SPICE-A5	0.994	6.76	10.00	0.33	3.33	0.12	2.84	0.32
SPICE-A6	0.972	7.47	8.89	0.31	3.59	0.14	3.17	0.34
SPICE-A7	0.983	7.51	9.54	0.35	4.36	0.14	3.92	0.33
SPICE-A8	0.999	12.01	7.24	0.22	2.99	0.12	2.48	0.32
SPICE-A9	1.061	7.63	8.55	0.29	2.65	0.12	2.01	0.31
SPICE-A10	0.978	4.77	12.50	0.50	3.27	0.10	2.82	0.33
10SPCO6	1.052	8.69	9.07	0.30	3.95	0.14	3.27	0.31
10SPCO7	1.071	7.07	9.85	0.34	3.49	0.12	2.79	0.30

Process blanks	Mass of synthetic quartz (g)	µg C [a]	$^{14}C/^{12}C$ (10^{-13}) [b]	2σ uncertainty (10^{-13}) [b]	^{14}C (10^3 atoms) [c]	2σ uncertainty (10^3 atoms)
CGN 40	3.054	6.33	0.86	0.13	27	4
CGN 47	1.003	18.03	0.53	0.06	48	6
CGN 48	0.996	9.32	0.57	0.08	27	4
CGN 49	2.999	12.03	0.72	0.07	44	4
CGN 106	0.495	13.12	0.87	0.08	57	6
CGN 107	1.015	19.76	0.75	0.06	74	6
CGN 108	1.000	10.34	0.89	0.12	46	6
CGN 109	3.014	4.97	2.09	0.31	52	8
CGN 124 [d,e]	2.047	13.06	1.12	0.09	73	3
CGN 130 [d,e]	3.542	5.53	2.13	0.33	59	5

Note: ^{14}C concentrations in this table are not scaled to sea level and high latitude (SLHL). All uncertainties are **2σ**.

[a] Amount of carbon in carrier added, the carrier was added as $CaCO_3$ (fragments of a '^{14}C-dead' Iceland spar; Fülöp et al. 2015)

[b] $^{14}C/^{12}C$ values are normalized using the OX-II standard (N.I.S.T designation SRM 4990 C). Uncertainty quoted is the counting uncertainty.

[c] The ^{14}C concentration is calculated from the $^{14}C/^{12}C$ concentration determined by AMS multiplied by the ^{12}C content of the sample (i.e. carrier + sample). The amount of C provided is the sum of carbon in the carrier and any carbon in the sample. The carbon amount is determined on a calibrated capacitance manomenter (calibrated with accurately weighed amounts of carrier), after cryogenic separation of CO_2 from other gases.

[d] Blank subtractions are between 1.7% to 2.2 % of the total ^{14}C measured. Uncertainties in the blank corrected ^{14}C concentrations include the propagated uncertainties in the total number of ^{14}C atoms in the sample and the uncertainty in the ^{14}C atoms in the blank, estimated from the mean and standard deviation of all blank measurements.

Table B4. *St*, *Sf*, and *Sa* scaling factors calculated for calibration sites on the SP lava flow.

	^{21}Ne, ^{10}Be, and ^{14}C	**^{21}Ne, ^{10}Be, and ^{14}C**	**^{21}Ne and ^{10}Be (over past 72 ka)**	**^{21}Ne and ^{10}Be (over past 72 ka)**	**^{14}C (over past 25 ka)**	**^{14}C (over past 25 ka)**	**^{10}Be (over past 72 ka)**	**^{10}Be (over past 72 ka)**	**^{14}C (over past 25 ka)**	**^{14}C (over past 25 ka)**	**^{14}C (over past 8270 yr)**	**^{14}C (over past 8270 yr)**	**^{14}C (over past 8270 yr)**	**^{14}C (over past 8270 yr)**
Sample ID	***St*** scaling factor for fast and slow muons [a]	***St*** scaling factor for neutron spallation [a]	***Sf*** scaling factor for fast and slow muons [b]	***Sf*** scaling factor for neutron spallation [b]	***Sf*** scaling factor for fast and slow muons [c]	***Sf*** scaling factor for neutron spallation [c]	***Sa*** scaling factor for fast and slow muons [b]	***Sa*** scaling factor for neutron spallation [b]	***Sa*** scaling factor for fast and slow muons [c]	***Sa*** scaling factor for neutron spallation [c]	***Sf*** scaling factor for fast and slow muons [d]	***Sf*** scaling factor for neutron spallation [d]	***Sa*** scaling factor for fast and slow muons [d]	***Sa*** scaling factor for neutron spallation [d]
SPICE-A1	1.993	3.515	1.506	3.861	1.498	3.602	1.506	4.021	1.498	3.582	1.490	3.522	1.490	3.498
SPICE-A2	1.965	3.445	1.496	3.777	1.488	3.524	1.496	3.931	1.488	3.505	1.480	3.446	1.480	3.423
SPICE-A3	1.968	3.452	1.497	3.786	1.489	3.533	1.497	3.941	1.489	3.513	1.481	3.454	1.481	3.431
SPICE-A4	1.962	3.436	1.495	3.766	1.486	3.515	1.495	3.920	1.486	3.495	1.479	3.437	1.479	3.414
SPICE-A5	1.959	3.430	1.494	3.758	1.485	3.507	1.494	3.911	1.485	3.488	1.478	3.430	1.478	3.406
SPICE-A6	1.938	3.379	1.486	3.697	1.478	3.451	1.486	3.847	1.478	3.432	1.471	3.375	1.471	3.352
SPICE-A7	1.959	3.430	1.494	3.758	1.485	3.507	1.494	3.911	1.485	3.488	1.478	3.430	1.478	3.406
SPICE-A8	1.939	3.380	1.486	3.698	1.478	3.452	1.486	3.848	1.478	3.433	1.471	3.376	1.471	3.353
SPICE-A9	1.968	3.452	1.497	3.786	1.489	3.533	1.497	3.941	1.489	3.513	1.481	3.454	1.481	3.431
SPICE-A10	1.959	3.430	1.494	3.758	1.485	3.507	1.494	3.911	1.485	3.488	1.478	3.430	1.478	3.406
10SPC01	2.031	3.609	1.520	3.974	--	--	--	--	--	--	--	--	--	--
10SPC06	1.958	3.427	1.493	3.755	1.485	3.504	--	--	1.485	3.485	1.477	3.427	1.477	3.403
10SPC07	1.946	3.399	1.489	3.721	1.481	3.473	--	--	1.481	3.454	1.473	3.396	1.473	3.373

Note: -- indicates a sample which was not analysed for the respective nuclide, and thus needs no scaling factor.

[a] The scaling factors were determined using CRONUSCalc (Marrero et al., 2016). Scaling factors are time independent.

[b] The scaling factors were determined using the mmc1 Matlab code of Lifton et al. (2014). Scaling factors are time-dependent. *Sf* scaling factors for ^{21}Ne and ^{10}Be and *Sa* scaling factors for ^{10}Be are integrated over the past 72 ka. There is no option for calculating Sa scaling factors for ^{21}Ne. *Sf* and *Sa* scaling factors for ^{14}C are integrated over the past 25 ka, the time at which ^{14}C reaches 95% saturation.

[c] *Sf* and *Sa* scaling factors for ^{14}C are integrated over the past 25 ka, the time at which ^{14}C reaches 95% saturation.

[d] *Sf* and *Sa* scaling factors for ^{14}C are integrated over the past 8270 a, based on the integration time equations 7 and 9 from Blard et al. (2019).

1430 Table B5. Local production-rate ratios and production-rate ratios for total reference ^{21}Ne and spallogenic $^{10}Be_{sp}$ and $^{14}C_{sp}$ in SP-flow
1431 quartz.

(a) Scaled with St scaling factors Sample ID	$^{21}Ne/^{10}Be$	2σ Uncertainty	$^{21}Ne/^{14}C$	2σ Uncertainty	$^{14}C/^{10}Be$	2σ Uncertainty	$^{21}Ne/^{10}Be_{sp}$	2σ Uncertainty	$^{21}Ne/^{14}C_{sp}$	2σ Uncertainty	$^{14}C_{sp}/^{10}Be_{sp}$	2σ Uncertainty
SPICE-A1	4.29	0.61	1.39	0.21	3.08	0.43	4.41	0.76	1.68	0.36	2.63	0.61
SPICE-A2	4.49	0.63	1.63	0.25	2.76	0.41	4.61	0.80	1.98	0.45	2.33	0.58
SPICE-A3	4.37	0.58	1.38	0.20	3.17	0.45	4.49	0.74	1.65	0.35	2.73	0.64
SPICE-A4	4.37	0.53	1.48	0.20	2.96	0.44	4.49	0.71	1.79	0.39	2.51	0.62
SPICE-A5	4.45	0.65	1.54	0.25	2.90	0.44	4.58	0.81	1.87	0.44	2.45	0.62
SPICE-A6	4.25	0.64	1.29	0.21	3.28	0.48	4.37	0.79	1.54	0.34	2.83	0.67
SPICE-A7	4.35	0.70	1.07	0.17	4.07	0.53	4.47	0.85	1.23	0.24	3.64	0.75
SPICE-A8	4.69	0.61	1.90	0.30	2.47	0.41	4.82	0.79	2.39	0.62	2.02	0.57
SPICE-A9	4.39	0.82	2.17	0.48	2.03	0.37	4.52	0.95	2.90	1.00	1.56	0.52
SPICE-A10	4.66	0.60	1.73	0.26	2.70	0.41	4.78	0.78	2.11	0.49	2.27	0.57
10SPC06	--	--	1.28	0.17	--	--	--	--	1.53	0.30	--	--
10SPC07	--	--	1.78	0.25	--	--	--	--	1.82	0.35	--	--

1432

(b) Scaled with *Sf* scaling factors								**(c) Scaled with *Sa* scaling factors**		
Sample ID	$^{21}Ne_{sp}/^{10}Be_{sp}$	2σ Uncertainty	$^{21}Ne_{sp}/^{14}C_{sp}$	2σ Uncertainty	$^{14}C_{sp}/^{10}Be_{sp}$	2σ Uncertainty		Sample ID	$^{14}C_{sp}/^{10}Be_{sp}$	2σ Uncertainty
SPICE-A1	4.41	0.76	1.64	0.34	2.94	0.65		SPICE-A1	3.08	0.68
SPICE-A2	4.61	0.80	1.93	0.41	2.61	0.62		SPICE-A2	2.73	0.64
SPICE-A3	4.49	0.74	1.61	0.33	3.04	0.68		SPICE-A3	3.19	0.71
SPICE-A4	4.49	0.71	1.74	0.36	2.81	0.66		SPICE-A4	2.94	0.69
SPICE-A5	4.58	0.81	1.82	0.41	2.74	0.66		SPICE-A5	2.87	0.69
SPICE-A6	4.37	0.79	1.51	0.32	3.15	0.72		SPICE-A6	3.30	0.69
SPICE-A7	4.47	0.85	1.21	0.23	4.01	0.80		SPICE-A7	4.20	0.84
SPICE-A8	4.82	0.79	2.30	0.56	2.28	0.61		SPICE-A8	2.38	0.64
SPICE-A9	4.52	0.95	2.74	0.88	1.79	0.55		SPICE-A9	1.88	0.58
SPICE-A10	4.78	0.78	2.05	0.45	2.54	0.61		SPICE-A10	2.66	0.64
10SPC06	--	--	1.49	0.27	--	--		10SPC06	--	--
10SPC07	--	--	2.15	0.45	--	--		10SPC07	--	--